GROWTH AND CHARACTERIZATION OF Sb_2Se_3 AND $SnSe_2$ CRYSTALS FOR PHOTOVOLTAIC APPLICATIONS

Synopsis submitted to CHRIST (Deemed to be University)

as partial requirement for the award of the Degree of

DOCTOR OF PHILOSOPHY

IN

PHYSICS

by

BIBIN JOHN

Under the Supervision of
Dr A G Kunjomana
Professor

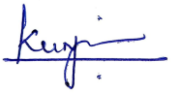

Name and Signature of Scholar

Name and Signature of Supervisor

CENTRE FORRESEARCH
CHRIST (Deemed to be University)

BENGALURU

MAY 2022

CENTRE FOR RESEARCH

Approval of PhD Synopsis

[as per clause 11(k.) of CU Regulation for the Degree of Doctor of Philosophy, May 2019]

Name of Scholar:	Bibin John
Department:	Physics and Electronics
Name of Co Supervisor:	Dr. A. G. Kunjomana
Names of Research Advisory Committee: 1. Dr. Bubbly S. G. 2. Dr. Imran Jafri R.	
Name and Designation of External Reviewer if applicable:	
Date of Synopsis Presentation:	15-05-2022
Title of the PhD thesis:	Growth and Characterization of Sb_2Se_3 and SnSe2 Crystals for Photovoltaic Applications

Approved by:

1. Name of Supervisor: Dr. A. G. Kunjomana Signature:
2. Name of RAC Member: Dr. Bubbly S. G. Signature:
3. Name of RAC Member: Dr. Imran Jafri R. Signature:
4. Name of External reviewer if applicable Signature:

Head of Department

Date of approval by Doctoral Committee:

Director Centre for Research

Table of Contents

Abstract

1 Introduction

2 Literature review

3 Objectives

4 Research work carried out

4.1 Growth and characterization of Sb_2Se_3 crystals

4.2 Growth and characterization of $SnSe_2$ crystals

5 Summary and future work

5.1 Summary of the research work

5.2 Scope for the future work

6 Plan of the thesis

Bibliography

Publications and Proceedings

Abstract

Tremendous development in crystal growth technology propelled the production of good quality samples for photovoltaic (PV) applications. In this regard, the present work emphasizes on the correlation between the synthesis, morphology, crystal structure and physical properties of binary layered chalcogenide materials (LCMs) like antimony selenide (Sb_2Se_3) and tin diselenide ($SnSe_2$). These compounds are gaining attention in the PV industry due to their eco-friendly, sustainable, and non-hazardous nature as well as the salient features such as moderate melting temperature, *p*-type with direct transition, optimum band gap and high absorption coefficient. Therefore, cost-effective synthesis was implemented to engineer bulk Sb_2Se_3 and $SnSe_2$ crystals for exploring the physical properties towards optoelectronic applications. Single crystal growth from melt allows relatively quick fabrication of large size samples compared to other techniques. However, it shows some disadvantages like difficulties in maintaining stable temperature for crystallization and achieving chemical homogeneity, especially in the case when multiple elements are present in the system. The complexities associated with Bridgman-Stockbarger and Czochralski methods for preparing bulk crystals include irregular heat flow, mechanical movement of furnace or crucible, thermal stress etc. Moreover, reactivity of the melted material with the ampoule leads to structural irregularities. Hence, horizontal normal freezing (HNF), the versatile and inexpensive synthesis technique, was employed to obtain large dimensional crystals. Most of the vapor growth methods, especially, the chemical vapor deposition (CVD) deteriorates the material quality and adversely affects the physical properties due to the presence of contamination or foreign elements. On the other hand, the physical vapor deposition (PVD) process is favorable as it offers feasible instrumentation and yields stoichiometric specimens with supreme quality and fine-tuned characteristics. The PVD method could provide the evolution of various habits under high vacuum if the processing protocols are critically controlled in a growth chamber. Even though research work has been published on Sb_2Se_3 and $SnSe_2$ samples prepared by other techniques, an economically viable approach by physical means for harvesting stoichiometric crystals, which enable versatile optical properties, has not been developed so far. A possible growth mechanism to explain the formation of crystals was proposed and discussed based on the Kossel-Stranski-Volmer (KSV) model. The phase identification, chemical homogeneity and microstructural evolution of the samples have been investigated by utilizing different sophisticated characterization tools like PXRD, EDAX, XPS,

optical microscope, SEM, and TEM. Thermogravimetric analysis was performed for accessing the melting temperature and thermal characteristics. Vickers microhardness tester was employed to probe the mechanical characteristics of the samples and Hall effect experimental setup was utilized to examine their transport properties. The optical measurements were carried out utilizing UV-Vis-NIR and PL spectrometers. The results obtained were analyzed systematically to assess the suitability of harvested products towards photovoltaic applications.

1 Introduction

Photovoltaics is an indispensable area of research for energy conversion, and its prime requirements include the choice of an eco-friendly absorber medium as well as the fine-tuning of material traits by proper control of synthesis protocols. In this regard, silicon (Si) based solar cell modules have been widely used by researchers, but due to feedstock problems, extensive purification is mandatory for the extraction of metallurgical to semiconductor grade silicon ingots, causing cost-intensiveness and high electric power consumption (Gibson,2019). Moreover, its high melting point (M.P = 1400 °C) complicates heat flow dynamics, which induces large dislocation density. Impurities such as carbon and oxygen introduced during growth can degrade the performance of Si solar cells by reducing their efficiencies. The presence of oxygen can create precipitates and act as recombination centers, which further shorten the lifetime of charge carriers. The indirect transition nature of Si with a low absorption coefficient inhibits the effective capturing of photons (Wu et al. 2008, Arnberg et al. 2012, Kivambe et al. 2017, Gibson. 2019). Therefore, it is inevitable to seek alternative compound semiconductors as most of those possess tunable optoelectronic parameters and complementary traits such that the thickness of the absorber layer can be made smaller than that of Si (Kunjomana et al. 2021). Sixth group chalcogen based materials stand out due to their economic viability and radiation resistivity. The compounds such as InP, GaAs, and PbSe have appreciable optical energy gap (E_g = 1.35-1.48 eV), absorption coefficient ($\alpha \sim 10^5$ cm^{-1}), resistivity ($\rho = 8 \times 10^7$ to 3.8×10^8 Ω cm) and carrier concentration ($n = 1.8 \times 10^6$ to 2×10^7 cm^{-3}) as reported by Oda (2007). The generation of photocurrent is effective in the prominent PV samples, (HgS/HgSe, CdSe/CdS, GaS/GaSe, and ZnS/ZnSe) which manifest a direct band gap with high absorption coefficient. As a result, experimental research has been widely focused on II-VI, III-VI, IV-VI candidates from the viewpoint of energy conversion applications (Afzaal and O'Brien. 2006, Oda. 2007). However, there are complexities associated with the hazardous nature of the constituent elements, Hg, Cd, Ga, and S in addition to the optimization of thermodynamic parameters (melting point, vapor pressure, Gibb's free energy, etc.), concerning synthesizability and chemical homogeneity (Oda. 2007, Kunjomana et al. 2021). Another constraint associated with polymorphism is evident in In_2Se_3 and In_2S_3 compounds, giving rise to the coexistence of different phases such as InS, InS_2, In_6Se_7, In_2Se_3, etc., which induce stoichiometric imbalance

and deteriorate the flow of charge carriers during the transport process (Rehwald and Harbeke. 1965, Ajayakumar and Kunjomana. 2016, Teena and Kunjomana. 2017). The difficulty of growing high-quality large single crystals prevented the development of many devices based on CdTe related materials because twin boundaries are easily formed owing to the very low stacking fault energy (Al-Hamdi et al. 2020). The crystals of group IV-VI (SnS, SnSe, $SnSe_2$) have also gained attention as they comprise fairly earth-abundant elements. SnS with E_g = 1.3 eV, $\alpha \sim 10^4$ cm^{-1} and tunable carrier densities ~ 10^{15} to 10^{18} cm^{-3} is effective for energy conversion, yet shows the existence of multiphase like SnS_2, Sn_2S_3, etc. (Reddy et al. 2006, Norton et al. 2021).

Compounds of the V-VI family, especially antimony selenide (Sb_2Se_3) bearing environmentally benign elements have received considerable interest owing to their notable physical properties. Layered atomic arrangement in the orthorhombic crystalline structure of Sb_2Se_3 leads to the formation of very few grain boundaries that help in reducing the recombination of light-generated charge carriers during the transport process. In addition, perspective features such as earth-abundant constituents (Sb and Se), suitable direct band gap ~ 1-1.3 eV, absorption coefficient ~10^5 cm^{-1} in the visible region (allowing most of the photons to be absorbed in a narrow depth), non-corrosiveness, and stability make *p*-type Sb_2Se_3, a potential candidate asa photon absorber medium in solar cells. Moreover, the Sb-Se binary system has only one stable phase, which is different from multi valence Cu-Se and Sn-Se binary systems. The components melt congruently at a moderate temperature in the ampoule as its M.P (611 °C) is low compared to CdTe (1092 °C) and GaAs (1238 °C), facilitating the chemical homogeneity of Sb_2Se_3 compound and its subsequent crystal growth. Furthermore, it does not decompose or segregate near the melting point, which helps to reduce the chances of the formation of a secondary phase. Thus, considering the advantageous intrinsic traits and distinct physical properties compared to the aforementioned materials, we focused on antimony selenide as it is well suited for photovoltaic applications. The right choice of synthesis method and processing protocols in an economically viable controlled environment is important to attain the desired size, shape, and purity of crystals, free of undesirable by-products (Nguyen. 1998, Vadapooet al. 2011, Liu et al. 2014, Tiwari et al. 2018, Liang et al. 2018, Mavlonov et al. 2020). Different physical and chemical approaches available to the bulk synthesis of Sb_2Se_3 have been published elsewhere (Rehwald and Harbeke. 1965, Reddy et al. 2006, Al-Ham et al. 2020, Nortonetal.

2021). Vadapoo et al. (2011) have reviewed the variation in the band gap of Sb_2Se_3crystals grown by zone refining, hydrothermal, Bridgman-Stockbarger technique, etc. Development of 3 cm long samples using the vertical Bridgman technique was accomplished by Hobson et al. (2018) following a growth period of 7 days and observed polycrystallinity in the region, 1.5-2 cm. Hence, these authors cleaved the single crystal part for structural and spectroscopic studies. Moreover, the sublimation process has also been employed but produces Sb_2Se_3 boules exhibiting rough surfaces and grooves with grain boundaries. Cone-shaped ingots bearing multi-grains and facets were detected after 14 days. Bacewicz and Ciszek (1991) carried out the liquid encapsulated synthesis of Sb_2Se_3 crystals and found surface defects. Wang et al. (2003) have grown whiskers by the addition of organic compounds to the hydrothermal system, which involved complex chemical reactions between the reagents ($C_4H_{10}O_3$ and H_2O), and thus were susceptible to non-stoichiometry.

Chemical vapor deposition (CVD) of tin selenide produced H_2Se, which is highly toxic (Boscher et al. 2008). Also, the occurrence of a chemical reaction or the movement of gases to the reaction zone by the aid of transporting agents prior to the growth causes contamination of the deposited materials. The synthesis process involves the adsorption of the reactant species catalyzed by the surface, desorption of the by-products, and incorporation of the condensed materials into the solid structures (Chattopadhyay and Banerjee. 2009). The exact growth mechanism of crystals via CVD is still elusive due to the transport process being controlled by gas supply, pressure gradient across the chamber, buoyancy of hot gases, and diffusionof vapors to the substrate. Another disadvantage is the slow-down of flow velocity near the crystallization region due to the viscous friction experienced by the gas molecules. Additionally, any defects in the CVD process deteriorate the optical, structural, and electrical properties of the samples, as reported by Tan et al. (2021). As such, the crystals grown by this method show inferior qualities, which adversely affect the physical properties, due to the presence of chemical impurities in the lattice structure. Chemical vapor deposition causes various challenges due to the utility of multiple precursors, including non-uniform distribution of as-grown domains, and numerous flaws and voids in the samples. Schoneich et al. (2010) conducted chemical vapor transport experiments in silica ampoules using iodine (I_2) as a carrier agent, yet lacked systematic work on characterization. The vacuum deposition of $As_2(Se, S)_3$ mixed compounds was carried out by

Smith et al. (1979) and emphasized that I_2 might have been incorporated in the lattice and therefore, solvents should be used to eliminate unwanted deposits from the surface. The inferiority of these crystals owing to the incorporation of foreign reagents poses problems in yielding desirable properties.

There is insufficient information in the literature regarding the control of physical vapor deposition (PVD) in a growth chamber to obtain the link between morphology, crystalline perfection and optical characteristics. The notable aspect of physical vapor deposition (PVD) is the production of defect-free stoichiometric crystals with diverse shapes and as-grown surfaces, which do not require cleaning, polishing, etc. that are commonly adopted for melt grown counterparts to meet the requirements of device fabrication. Also, the PVD process offers relatively simpler as well as economically viable instrumentation and yields nearly perfect, monophase solids compared to CVD. It allows the evolution of different habits without the need of seed or foreign reactants if the processing protocols are controlled critically in a synthesis chamber under high vacuum. Moreover, PVD yields physically distinct and chemically homogenous samples from the nutrient phase devoid of elemental traces. In the PVD method, it is necessary to systematically steer the interrelated experimental aspects such as geometry of ampoules, source materials, growth conditions, temperature profile and kinetics of crystallization. Therefore, we developed a cost effective PVD process for the bulk production of stoichiometric Sb_2Se_3 crystalline habits, by systematically controlling the solidification environment, limiting the mass transfer of the diffused vapor species and eliminating the stringent conditions as well as contaminations. Reports are meagre dealing with the experimental methodology for the kinetic generation of coir-like fibres, whiskers, needles, spherulites, etc. as well as the effect of morphology on the structural quality of vapor deposited Sb_2Se_3. Hence, the present research work aims at shape evolution of the as-grown crystals without the utilization of seed or foreign precursors by the production of symmetrical crystalline habits with superior physical properties towards the enhancement of device performance. The platelets and needles of arsenic, antimony and bismuth chalcogenides were deposited by Arivuoli et al. (1988), which showed deficiency in chemical homogeneity. The inferiority of these crystals owing to the incorporation of foreign reagents poses problems in yielding desirable properties. Bibin and Kunjomana (2019) could synthesize tiny crystalline habits of antimony

selenide by sublimation process under low mass transfer. Aggregates were found due to multiple nucleation associated with the improper control of growth conditions and prone to slightly off-stoichiometry as raw antimony selenide was vaporized in the ampoule. Therefore, a two-step process involving customization of chemically homogeneous Sb_2Se_3 precursor has been implemented and subsequently, bulk crystallization was accomplished under regulated vacuum atmosphere (without the use of any foreign chemical transporting agents). Band gap engineering of different growth forms was made possible in order to understand the structure-morphology-property relationship. Special attention has been paid to facilitate progressive vapor-solid (v-β) transition by maintaining slow cooling in order to avoid rapid phase transition and facilitate high degree of crystallinity. More importantly, optimization of supersaturation to get stoichiometric and mechanically strong whiskers with favourable physical properties towards the enhancement of photovoltaic performance is explored for the first time. Appreciable degree of internal periodicity of the crystalline lattice was accomplished by optimizing the processing conditions, so as to enable desirable material traits of the grown crystals, considering their functional perspective as absorbers for PV applications.

Bhatt et al. (1989) have prepared the homogeneous $SnSe_2$ compound filling stoichiometric proposition of tin and selenium of 99.99% purity in a quartz ampoule of dimensions, 25 cm in length and 1.2 cm in diameter and sealed under a vacuum ~10^{-5} mbar and this ingot was utilized for crystal growth by the Bridgman-Stockbarger technique, subjecting to a lowering rate of 4 mm/h. Though the samples were reported to have a reasonable perfection, their cleaved surfaces exhibited indirect transition with band gap of 1.01 eV. The same method followed by successive re-crystallizations has been employed for the study of morphology, chemical composition and mechanical strength, as per the reports of Trifonova and Yanchev (1996),which produced crystals of size, ~10 × 10 × 1 mm^3, (bearing grey metallic colour and pronounced layered structure) with starting materials, 99.9999% pure Sn and 99.99% pure Se. The harvested products had maximum deviation ~4% from the ratio based on the molecular formula, Sn_xSe_2, (x =1). The compositional analysis showed, x > 1, indicating that during growth of the crystal, excess Sn had incorporated in the crystal lattice. Powell and Grant (1977) have grown $SnSe_2$ crystals with the dimension of 2 × 2 × 0.2 $cm^3$and thickness of 0.05 cm by a vertical Bridgman furnace. The grown crystals were easily cleaved perpendicular to the *c*-axis

using a razor blade and determined the *6H*-polytype. Other tin diselenide crystals grown by iodine vapor transport were found to be *2H*, but tended to grow only in thin plates. The thicker crystals grown by the melt method were of mixed polytypes. The direct band gap values disagree with those previously reported, the discrepancy being much more than that due to polytypism. Anh Tuan Pham (2021) has grown $SnSe_2$ single crystals by the temperature gradient method using the high purity (5N) Se and Sn powders with the molar ratio of 2:1 were weighed and vacuum-sealed (< 10^{-4}Torr) in quartz ampoule. But, sublimation process offers a flexible approach for the yield of ordered solids from the gaseous phases. Tin diselenide single crystals were grown by George and Kumari (1986) using the physical vapor transport (PVT) method from the stoichiometric ingot by maintaining the source and growth temperatures at 640 °C and 500 °C, respectively, and the transport time was around 100 h. The crystals obtained are in the form of platelets having thickness < 150 μm and surface area. The quartz ampoules of 15 cm length and 1.6 cm inner diameter were used for the synthesis. In order to reduce the large number of nucleation sites in the ampoule, these tubes were cleaned thoroughly by washing first with detergent soap solution, then kept in aquaregia for 2 to 3 h, washed and cleaned ultrasonically with doubly distilled water and acetone. The tube was then evacuated to about 10^{-5} Torr and flame heated for half an hour. Circular and hexagonal spirals have observed on the as-grown faces of the $SnSe_2$ crystals by the spiral growth mechanism. Agarwal et al. (1991) reported that the bulk $SnSe_2$ compound prepared from stoichiometric amount of Sn and Se were sealed in a an evacuated quartz ampoule and slowly heated over the period of 5 h to a temperature of nearly 500 ºC for 24 h and then allowed to cool to room temperature in gradual steps. The shining polycrystalline mass were thoroughly vibrated for about 30 min to ensure the proper mixing of the contents, and have been utilized for the growth of single crystalline $SnSe_2$ crystals by direct vapor transport in an etched and vacuum backed ampoule (230 mm long, with inside diameter ranging from 15 to 30 mm) at a reaction zone temperature of 410 ºC. Garg et al. (1976) carried out vapor phase transport technique without using a transport agent for the $SnSe_2$ crystal growth. The polycrystalline ingot was prepared by melting the stoichiometric amount of high pure component materials in an evacuated transparent silica ampoule, about 20 cm in length and 2 cm in diameter. Rapid cooling resulted in a mixture of SnSe and $SnSe_2$ due to the considerable dissociation of $SnSe_2$. The growth habits were found to be hexagonal platelets of 0.5 mm thick and 1 cm^2 surface area. The crystals possessed *n*-type electrical conductivity with

a carrier concentration of 10^{17} cm^{-3}, due to the contribution to the selenium deficiency. Crystals of layered compounds grown by CVT in quartz ampoules with 0.1 g of iodine was discussed by Rimmington and Balchin (1972). The harvested products comprised precipitates, which were detected on the surface of the specimen using optical microscopes. The precipitates were richer in tin and iodine than the surrounding matrix, indicating off-stoichiometry. Minagawa (1980) have synthesized hexagonal plates of $SnSe_2$ by chemical transport reaction using iodine as the transporter at a very low ΔT = 20 ºC by adjusting the temperature of reaction and growth zones at 590 ºC and 570 ºC, respectively. However, structural polytypism was examined, deteriorating the performance of the crystallized samples. Acharya and Srivastava (1981) have grown $SnSe_2$ crystals by iodine vapor transport technique at a temperature difference of 100 ºC (reaction zone = 530 ºC and growth zone = 430 ºC) employing a horizontal two-zone gradient furnace. The ingot together with a small amount of iodine (5 mg/cm^3 of the volume) was placed in an evacuated and sealed quartz ampoule of length 20 cm and diameter 16 mm. The $SnSe_2$ crystals obtained were shining black hexagonal plates, with lateral dimensions ranging from one to a few mm and thickness from 10 to 200 μm. In view of these considerations, physical vapor deposition of antimony and tin diselenide crystals was carried out in a thoroughly cleaned ampoule under high vacuum by subliming the customized stoichiometric ingot and was characterized for photovoltaic applications.

2. Literature review

Various aspects related to the methodology of crystal growth such as synthesis procedure, ampoule design, instrumentation, subsequent physical and chemical characterization techniques were reviewed systematically with the help of existing scientific reports and standard textbooks. Thorough literature survey enabled an up-to-date knowledge of the current research trend in the field of materials science, which provided a comprehensive understanding of the processing-structure-property relationship in the case of chalcogenide materials. Silicon (Si) and germanium (Ge) are the most commonly used elemental semiconductors in optoelectronics. However, they have low absorption coefficient (α) and exhibit an indirect band gap of 1.12 eV and 0.66 eV, respectively; whereas, tin (Sn), which is also a IV group material, possesses a low optical band gap (E_g) of 0.08 eV. All these elemental semiconductors have a diamond crystal structure. On the other hand, compound semiconductors have gained immense attention because

of their superior optoelectronic characteristics compared to those of elemental materials (Si and Ge). In this aspect, the binary semiconductors can be obtained by combining the elements of the following groups; II-VI, III-V, III-VI, IV-VI, and V-VI. The II-VI semiconductors such as ZnS, ZnSe, ZnTe, CdS, CdSe, and CdTe have high E_g values ranging from 1.56–3.68 eV. These chalcogenide materials have a direct nature of transition, high absorption coefficients and showcase a zinc-blende structure. However, there are concerns regarding the environmental issues due to toxicity which hinder their usage. The growth method and physical properties of elemental as well as compound semiconductors were presented in Table 1.

Group IV-VI compounds such as, SnS and SnSe have direct E_g (1 to 1.4 eV) with appreciable α. However, some of the materials such as P, Ga, As, S, Pb, and Te, belonging to these groups, are scarce, expensive, and hazardous. Other IV-VI group semiconductors like SiC have wurtzite structure and indirect band gap (2.99 eV). Si_xGe_{1-x} alloys have a zinc-blende structure with high absorption coefficient. Their implementation however is limited due to high melting temperature and complexity caused by in-homogeneity (Oda. 2007). In this regard, it is quite interesting to note that a considerable amount of research has been focused on groups IV-VI and V-VI layered semiconducting compounds owing to tunable optoelectronic properties. Binary chalcogenides like Sb_2Te_3, Sb_2S_3, and Sb_2Se_3 materials belong to group V-VI. These are also good thermoelectric compounds due to the high Seebeck coefficients and power factors. Among these binary semiconductors, the diverse morphological forms of Sb_2Se_3 and $SnSe_2$ layered materials have attained special interest attributed to the tunable band gap (1-2 eV) with a high absorption coefficient (~ 10^{-5} cm^{-1}). Moreover, these materials have optimum mobility, carrier concentration and low resistivity. Diverse morphological forms of these compounds are to be studied for improving their characteristics. Most of the compound semiconductors have a direct band gap with a higher absorption coefficient and consequently, the thickness of the absorber layer is lesser than indirect transition materials. These attributes promote compound semiconductors as promising materials for solar cell applications. Based on literature reviews, the current research work is focused on the growth of $SnSe_2$ and Sb_2Se_3 compounds, owing to their novel optoelectronic characteristics, suitable for photovoltaic energy conversion.

Table 1: The processing protocols, crystal structure, optical and electrical parameters of the prominent elemental and binary compound semiconductors

Sample	Melting Point (°C)	Growth Method	Crystal structure	Nature of transition	Optoelectronic properties			
					E_g	ρ	μ	n
					eV	Ω cm	$cm^2V^{-1}\ s^{-1}$	cm^{-3}
Elemental semiconductor								
Si (Oda, 2007)	1410	Czochralski	Diamond	Indirect	1.10	3.2×10^5	450	2.8×10^{19}
Ge (Oda, 2007)	937	Bridgman	Diamond	Indirect	0.66	....	1900	....
Compound semiconductor								
Group II-VI compounds								
CdTe (Oda, 2007)	1092	Bridgman	Zinc blende	Direct	1.49	....	100	$\sim10^{17}$
CdSe (Oda, 2007)	1239	Bridgman	Wurtzite	Direct	1.74	1×10^3	50	6×10^{13}
Group III-V compounds								
GaAs (Oda, 2007)	1238	Liquid encapsulate Czochralski	Zinc blende	Direct	1.43	3.8×10^8	420	2.1×10^{16}
GaSb (Oda, 2007)	712	Liquid encapsulate Czochralski	Zinc blende	Direct	0.70	....	1400	$\sim10^{14}$
Group III-VI compounds								
InSe (Teena et al. 2018)	611	Vapor growth	Hexagonal	Direct	1.45	1.7×10^2	11.14	1.5×10^{20}
In_2S_3 (Zhang et al. 2018)	420	Vapor growth	Tetragonal	Direct	1.37	….	17.6	$\sim10^{18}$
Group IV-VI compounds								
SnSe (Kunjomana et al. 2019)	880	Bridgman	Orthorhombic	Direct	1.30	….	….	$\sim10^{17}$
SnS (Hegde et al. 2011)	880	Vapor growth	Orthorhombic	Direct	1.30	120.35	34.14	1.5×10^{15}
$SnSe_2$ (Julien et al. 1987)	650	Bridgman	Hexagonal	Direct	1.21	1.6	67	$\sim10^{16}$
Group V-VI compounds								
Sb_2S_3 (Liu et al. 2016)	550	Chemical vapor transport	Orthorhombic	Direct	1.60	1.3×10^8	6.4	7.3×10^{13}
Sb_2Se_3 (Bacewicz& Cizek. 1991)	611	Bridgman	Orthorhombic	Direct	1.20	17	36	$\sim10^{18}$

The performance of devices depends on the purity, perfection, and homogeneity of the employed crystals which in-turn depends on the growth method. Hence, appreciable improvements have been made in crystal growth technology concerning uniformity, reproducibility, mechanical, thermal stability, size, and impurity control. Presently, many growth methods for bulk crystals have been developed. Though advanced techniques like Czochralski crystal-pulling, vertical Bridgman-Stockbarger (VBS) technique, zone refining, chemical vapor transport (CVT), chemical vapor deposition methods, etc. have emerged, they face challenges with regard to the production of good quality crystals. Additionally, these are cost-intensive and consume high amounts of electric power. Bletskan (2007) reviewed the preparation of chalcogenide crystals using the Czochralski method and reported that maintaining stoichiometry of the melt was challenging. Many research groups have discussed the difficulties associated with the aforementioned growth methods due to high temperature or pressure. Hence an intense literature review based on crystal growth facilitates the selection of a feasible synthesis approach. Various techniques, mainly classified into solution, melt and vapor growth methods, aimed at growing single crystals have been revised. The solution growth refers to obtaining crystals from a supersaturated solution of its constituents. It is widely utilized to prepare oxide based crystals and largely influenced by the composition of the solution. A significant change in the composition adversely affects the grown crystal. The growth rate is also significantly low. On the other hand, in melt growth, the source material is first melted at high temperature and subsequently supercooled to initiate crystallization. It is concerned specifically with the growth of congruent or near congruent melts. The material decomposes before melting or melts incongruently; it sublimes directly or its vapor pressure is too high at the MP. It is impractical to use this method for synthesizing compound crystals which have high melting points. However, in vapor growth, the starting material (compound melt only at the elevated pressure) is sublimed either in a vacuum environment, a stream of carrier gas or vapor of its constituents for crystallization. Economically viable synthesis strategies can be applied for the growth of $SnSe_2$ and Sb_2Se_3 with diverse morphological structures.

Czochralski growth method is mainly used for the industrial production of silicon wafers. A single crystal seed is attached to a pulling rod, this seed material is dipped in the molten feed in a crucible which simultaneously rotates and elevates. As a result single crystals are

synthesized. This method has the merits like high growth rate and production of large diameter crystals. Even though this method can yield large size crystals, the rotation, pulling, and seed material can cause contamination or high dislocation in the final products. This method is applied only to a limited number of compound semiconductor materials such as GaSb and InSb. While considering the Bridgman-Stockbarger method, the basic concept of this synthesis process is that the whole charge is molten and then solidified from one end. The materials to be crystallized are usually contained in a cylindrical crucible, which is lowered into a temperature gradient. The tip of the crucible is conical and hence initially a small volume of the melt is supercooled. Thus only one nucleus originates at the tip of the ampoule. If the nucleus is suitably oriented it may dominate the growing interface. In this melt growth, the motion of the ampoule is essential and should be slow and steady. This can be achieved by the use of wires and pulleys. To obtain constant speeds it is desirable to use a servo motor system or a constant speed motor, with variable gear ratios if a range of speed is required. Even though this method can produce single crystals, the translation and rotation of the ampoule will induce high dislocation and structural disorders. Hobson et al. (2018) have grown bulk crystals of antimony selenide (3 cm long) through the vertical Bridgman method. The synthesized materials were found to be polycrystalline. Bhatt et al. (1989) have harvested single crystals of $SnSe_2$ by the Bridgman technique. Though the crystals had a large size, the main problem associated with this method was high dislocation density ~10^5 cm^{-2}. In the float zone technique, the polycrystalline feed rod is melted by a zone heater and this melted zone can be held as it is because of the capillary force of the melt without touching any container material. Since the melt is not in contact with any furnace, high-quality materials can be grown without any impurities from the furnace material. The horizontal normal freezing (HNF) is based on a directional solidification of the melt by decreasing the melt temperature, i.e. the solidification of the charge from one end. It involves no mechanical movement of the crucible or furnace and hence, there is no mechanical vibration during the growth process. In the HNF method, the material is sealed in an ampoule and melted at a temperature higher than the melting point. The ampoule is not moved and the temperature distribution is changed as the crystal is grown from the sealed end.

In the vapor growth method, the growth temperature is reduced using a transport medium or carrier gases such as iodine, oxygen, etc. This approach is known as chemical vapor transport

(CVT) method. However, it is very difficult to control the speed of gases during the growth, which affects the growth mechanism. It involves a complex carrier gas transport process which results in the formation of byproducts or impurities. Thin $SnSe_2$ single and polycrystalline platelets were prepared by Domingo et al. (1966) using chemical (iodine) vapor transport method, but the obtained samples were contaminated due to the carrier gases. Grown platelets were in cluster form along the walls of the tube and hence the samples exhibited inferior characteristics. Polycrystalline $SnSe_2$ structures were synthesized through direct vapor transport with a small amount of carrier gas (iodine) and possessed higher electrical properties than their melt-grown counterparts (Agarwal et al. 1989). Agarwal et al. (1991) have grown layered $SnSe_2$ samples, employing direct vapor transport method, but the materials showed traces of iodine. Agarwal et al. (2007) produced tin diselenide crystals using chemical vapor transport technique. However, the habits showed anisotropy in electrical resistivity because of the existence of stacking faults. Large-scale production, reproducibility, and high growth rate are possible in chemical vapor deposition (CVD). But this method involves the presence of corrosive gasses, which may contaminate the sample. Therefore, additional cleaning is necessary for the harvested products. It is also difficult to control the vapor flow as the uncontrolled carrier gas transport may lead to defects/imperfections in the crystals. On the other hand, when materials were kept at a high temperature, the vapors were transported to the growth zone under a concentration gradient and were deposited on the walls of the ampoule (substrate) after particle diffusion. This yielded nearly perfect crystals with high mechanical strength. Crystallization in different morphological forms such as rod, wire, whiskers, needles, platelets, and spherulites is possible through physical vapor deposition (PVD) method. As such, the present research work emphasizes the engineering of good quality antimony and tin selenide crystals for obtaining superior optical and electrical properties for PV applications. The literature review aided in finalizing the research problem, which is focused on the growth of good quality Sb_2Se_3 and $SnSe_2$ crystals, employing physical vapor deposition (PVD) and horizontal normal freezing (HNF) methods. X-ray diffractogram (XRD) is a fingerprint technique used to probe the internal atomic arrangement such as lattice parameters, cell volume, density, etc., and the monophase nature of the grown crystals. Energy dispersive analysis by X-rays (EDAX) and X-ray photoelectron spectrometers are efficient tools to investigate stoichiometry, atomic ratio, and impurity contents. The optical and electron microscopes are effective to study the micro-

structure and growth mechanism of the crystal surface. Microhardness tester and thermogravimetric analyzer are simple techniques to test the hardness parameters and the temperature stability. UV-Vis-NIR and photoluminescence spectrometers are the popular tools to measure optical parameters like band gap, absorption coefficient, absorption, reflection, etc. A conventional hot probe and Hall effect setup are the commonly used experiments to measure the electrical parameters. Hence, the research work is focused on the growth of good quality Sb_2Se_3 and $SnSe_2$ crystals, employing physical vapor deposition and horizontal normal freezing methods. The experimental work also aims to investigate the morphology, growth mechanism, structural, optical, and electrical properties using optical and electron microscopes, XRD, UV-Vis-NIR, PL and Hall effect technique to explore their novel characteristics for photovoltaic applications.

Statement of the research problem

The present research work emphasizes the growth and characterization of Sb_2Se_3 and $SnSe_2$ crystals for photovoltaic applications. It deals with the systematic studies on the correlation between synthesis-morphology-structure-properties-performance of the grown samples by vapor and melt growth methods

3. Objectives

The present research work emphasizes on the growth and characterization of Sb_2Se_3 and $SnSe_2$crystals by physical vapor deposition (PVD) and horizontal normal freezing (HNF) methods for photovoltaic applications.

- To grow stoichiometric crystals of Sb_2Se_3 and $SnSe_2$ by physical vapor deposition (PVD) and horizontal normal freezing (HNF) methods
- To elucidate the structure, phase, morphology, growth mechanism, composition and melting temperature of the grown samples by employing the characterization tools such as XRD, EDAX, XPS, SEM, AFM, TEM, TGA, chemical etching, etc.
- To evaluate the mechanical strength and stability with the aid of micro indentation analysis

- To study optical properties of the grown samples utilizing UV-Vis-NIR spectrophotometer and photoluminescence spectrometer as well as electrical properties by employing Hall effect and I-V measurements for solar cell applications

4 Research work carried out

4.1 Vapor growth of Sb_2Se_3 crystalline habits

Bulk crystallization involves the birth of a nucleus and subsequent development of a periodic solid due to a driving force (supercooling in melt growth and supersaturation in solution/vapor growth) causing the system to evolve from its equilibrium. The morphology of a crystal governs the physical properties and is determined by the inherent crystal structure and growth conditions (Sunagawa. 2005). Therefore, the correlation between these internal and external factors have been explored to engineer stoichiometric Sb_2Se_3 crystals, by vapor deposition technology in a controlled environment with the aid of an indigenously fabricated horizontal dual zone furnace and a specially designed (15 × 17 mm diameter) ampoule employing high vacuum, (~10^{-6} mbar). Table 2 shows the growth conditions employed for the vapour deposition of Sb_2Se_3crystals by critically fine-tuning the experimental protocols.

Table 2: Growth conditions for Sb_2Se_3 crystals

Temperature (^oC)		Temperature difference ΔT (^oC)	Morphology of Sb_2Se_3 crystals
Nutrient zone T_N	Substrate zone T_G		
690	560	130	Fibres
680	590	90	Rods
650	580	70	Octahedra
630	570	60	Spheres

Teena & Kunjomana (2018) have discussed the pathways for the evolution of polycrystalline morphology to harvest bulk indium mono-selenide (InSe) morphologies such as needles, platelets, and spherulites with a progressive increase in mass transfer, but the information regarding the growth kinetics of low dimensional habits was not explored. Hence, in the present work, for the accomplishment of novel optical characteristics, special attention has been paid to focus on low dimensional sample crystallization, by reducing ΔT from 130 to 60 °C, keeping the extrinsic variables, T_N and T_G as constant, such that the diffusion of vapors from the nutrient

phase was controlled by limiting the degree of concentration gradient. The non-equilibrium state constituted by the excess of pressure (p) at the substrate zone, p, over the equilibrium vapor pressure, p_e (Supersaturation, $S = \frac{p-pe}{pe}$) led to the development of clumps of Sb_2Se_3 fibres of a few millimeters long (~10 mm) with 1 to 2 μm^2 cross-section, corresponding to ΔT = 130 °C. Similar kind of microfibers was observed in the physical vapor deposited InSe crystals (Teena & Kunjomana, 2018). The particular feature of interest of the as-grown Sb_2Se_3fibers is impeded growth with fast crystallization along the *c*-axis, inhibiting growth along the other two directions because the side faces are of low energy exhibiting stable configuration. The rough interface commonly comprises a larger number of kinks than the smooth interface and hence causes surface irregularities with non-uniformity in chemical composition. In the present work, the formation of good quality fibers implies that the proposed growth mechanism of Sb_2Se_3 follows the advancement of atomically smooth vapor (V)-solid (β) interface with accompaniment in the change in energy ($G_V - G_\beta$). The nucleation stage is complete once the embryo attains a critical size (r*) and the commencement of growth stages purely depends on the decrease in free energy between the two phases. Due to the periodic incorporation of constituent building units, the growth of faces was completed as per the Kossel, Stranski, and Volmer (KSV) growth mode (Sunagawa, 2005).As the microfibers grow from the tip, steps and kinks (marked in Fig. 1(d)) were evolved parallel to that of bulk crystals. When the sides with high lattice density that bind the fibers have already accomplished a decrease in the latent heat of crystallization, the degree of disordering of atoms will be reduced by the addition of atoms to kinks at the tip, overcoming the activation energy barrier, (ΔG^*). The probability of capturing atoms at the kink sites is higher than the surface terrace in accordance with the formulations of KSV model and the successive growth was facilitated due to layer by layer addition with the aid of two-dimensional (2D) nucleation by eliminating high energy surfaces (Kunjomana et al., 2015). The microcrystals were grown in bundles due to multiple nucleations, which arose from the perturbation of vapor flow at enhanced nutrient temperature, T_N. Hence, the deposition conditions were intentionally tailored to yield small sized structures. When T_N was decreased from 690 to 680 °C, rods were formed (Fig. 1a).

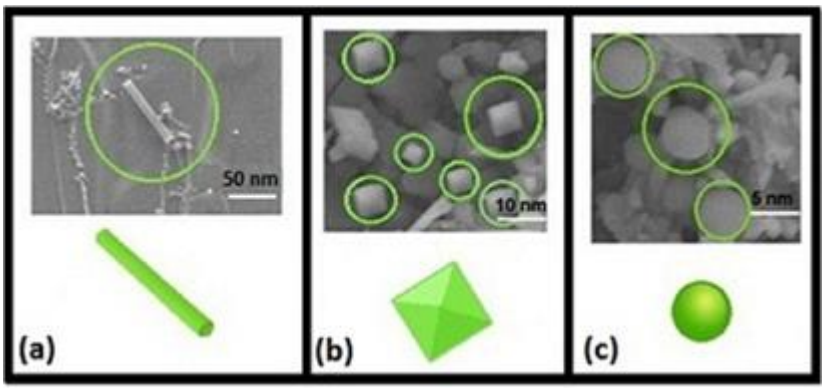

Fig. 1: Morphology of (a) rods (b) octahedra and (c) spherical-shaped crystals.

The TEM images (Fig. 2a-b) revealed the surface topography of the as-grown Sb_2Se_3rods of length~100-500 nm (see Fig. 3). The measured diameter of these crystals (~50 nm) was found to be less than that reported by Ma *et al*. (2009). The one-dimensional rods were grown along the [001] axis, due to the inherent layered orthorhombic crystal structure of Sb_2Se_3 (Tideswell*et al.,* 1957) consisting of atomic layers stacked in the order, *Se-Sb-Se-Sb-Se-Se-Sb-Se-Sb-Se,* which is analogous to the intrinsic mechanism proposed by Zhao *et al*. (2007). In agreement with their research findings, during the process of nucleation and growth, the crystallization rate is faster along the *c*-axis than the other two axes. The lattice comprises Sb and Se atomic chains parallel to the *c*-axis, which is the rod axis of the present as-grown rods as reported by Tideswell et al. (1957). The strongest bonds are within the chains, wherein, the Sb-Se distance ranges from 2.576 Å to 2.777 Å. The chemical bonding between Se-Se layers is provided by weak van der Waals forces and is positioned at 2.98 Å. The appearance of steps and kinks (marked in Fig. 2a), is similar to that of microfibers. The enhanced stacking of atomic layers at the tip under optimized supersaturation (*S*) facilitated space filling so as to form uniform rod (Fig. 2b), which provides the basis for layer growth mechanism based on the KSV theory of nearly-perfect crystals. There are no signs of growth features such as twisted or ramped atomic steps, helical patterns or spirals, hillocks *etc*. which establishes the absence of screw dislocation mechanism. HRTEM image and SAED pattern of the region marked in Fig. 2b are displayed in Fig. 2c-d. Figure 2c mirrors lattice strips of the rod with spacing, 0.826 nm, which is a value close to the interplanar distance of the (110) planes of Sb_2Se_3. Crystal periodicity leads to diffraction spots as manifested by the reciprocal lattice points of the image (Fig. 2d).

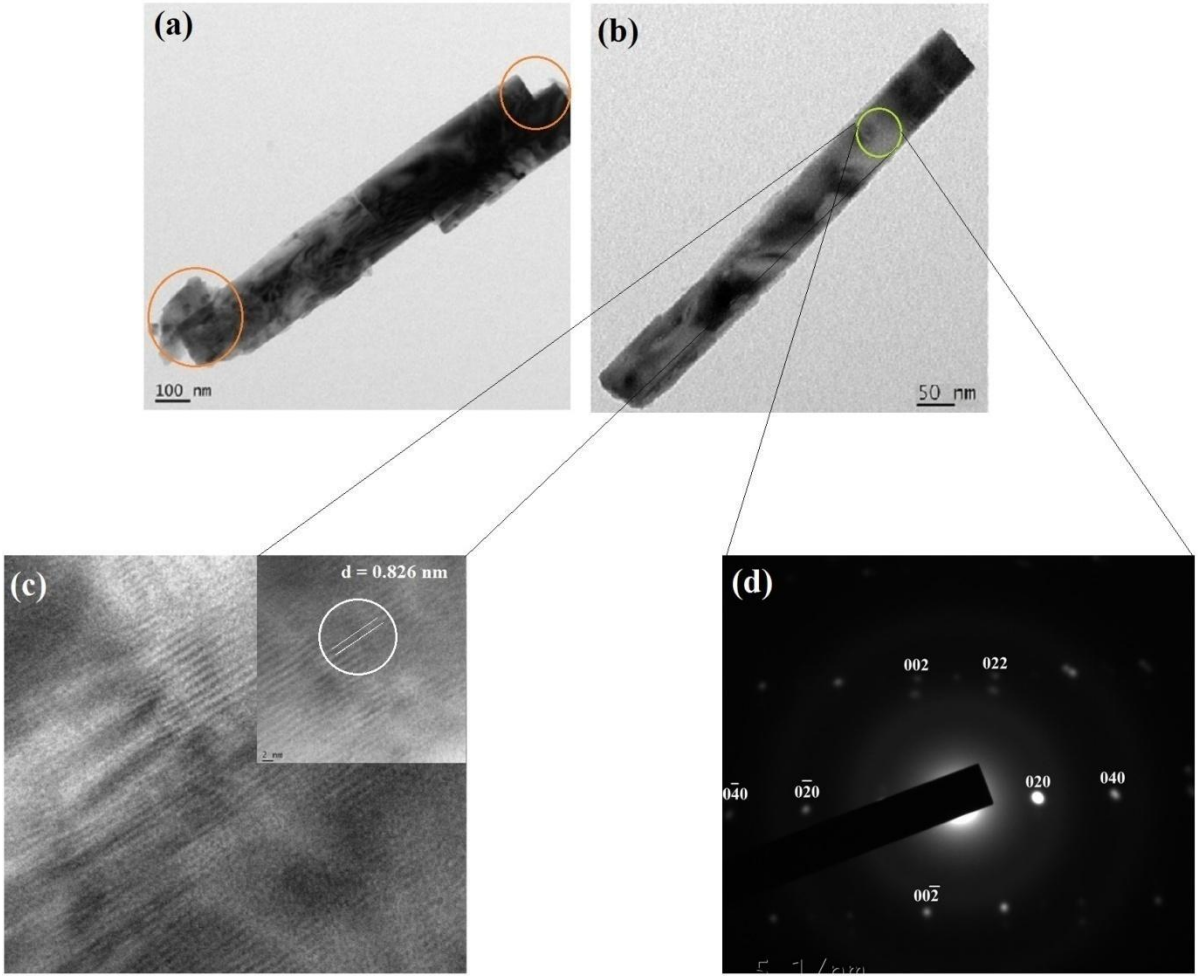

Fig. 2: TEM images of (a) Sb_2Se_3 rod showing steps and kinks; (b) completely grown uniform rod; (c) HRTEM images of the rod; (d) SAED pattern.

Further decrease in T_N could yield octahedral and nearly-spherical nanostructures (NS) as schematized in Fig. 1 (b-c). Xia *et al.* (2009) have reviewed the chemical reduction route for the preparation of octahedra with citric acid as a reducing agent and capping agent at a high concentration of Pd precursor, for which the shape is analogous to that of depicted in Fig. 1(f). Low dimensional crystal growth with polyhedral morphology was thermodynamically facilitated by the kinetic factor, Gibbs free energy, as a function of ΔT, according to the expression (Teena & Kunjomana, 2018, Pamplin, 1975).

$$\Delta G = -\frac{\lambda (T_N - T_S)}{T_N} = -\frac{(\lambda \Delta T)}{T_N} \quad (1)$$

The degree of driving force (supersaturation) plays a significant role in governing the nanostructure habit evolution, as it depends on the difference in chemical potential of nutrient and solid phases in the form, $\Delta\mu = \mu_N - \mu_S$, which can also be expressed by,

$$\Delta\mu = kT \ln \frac{P\text{-}P_e}{P_e} = kT \ln S \quad (2)$$

When ΔT was reduced to 60 °C, mass transfer was restricted facilitating a decrease in $\Delta\mu$ proportionate to concentration gradient. Hence spheres were formed with minimal change in free energy, compared to other geometrical shapes (Teena & Kunjomana, 2018 and Sunagawa, 2005). The typical equilibrium morphology was thus determined by the restricted mass transfer from the host stoichiometric charge with a decrease in T_N (630 °C). Sb_2Se_3 crystals were grown due to vapor-solid transition in concurrence with the KSV model. Similar growth mechanism was reported by Yin & Wang (2016) for the large-scale production of ZnO wires having hexagonal structures under argon atmosphere, employing high system temperature. Though this study concerns with kinetic control on growth over polycrystalline alumina substrates, insight for the evolution of pheres was not precisely discussed. The vapor-solid approach for the fabrication of few-layer graphene (FLGs) on carbon tubes and Si wafers was reported by Deng et al. (2012) without the use of a catalyst. In this case, the growth mechanism was guided by the nucleation of small-scale point defects and subsequent formation of large-scale linear defects. On the other hand, it is worthwhile to point out that the predominant shape of PVD grown Sb_2Se_3 crystals was achieved by enhancing the vacuum of growth chamber, critically controlling the population of adatoms to be deposited on the substrate and optimizing the mass transfer operations, without the use of foreign precursors or seeds and hence unlikely to pick up imperfections in the crystalline lattice. The externally applied thermal parameters such as the temperatures, T_N and T_G were precisely controlled to favor the right thermodynamic conditions for the vapor growth of crystals.

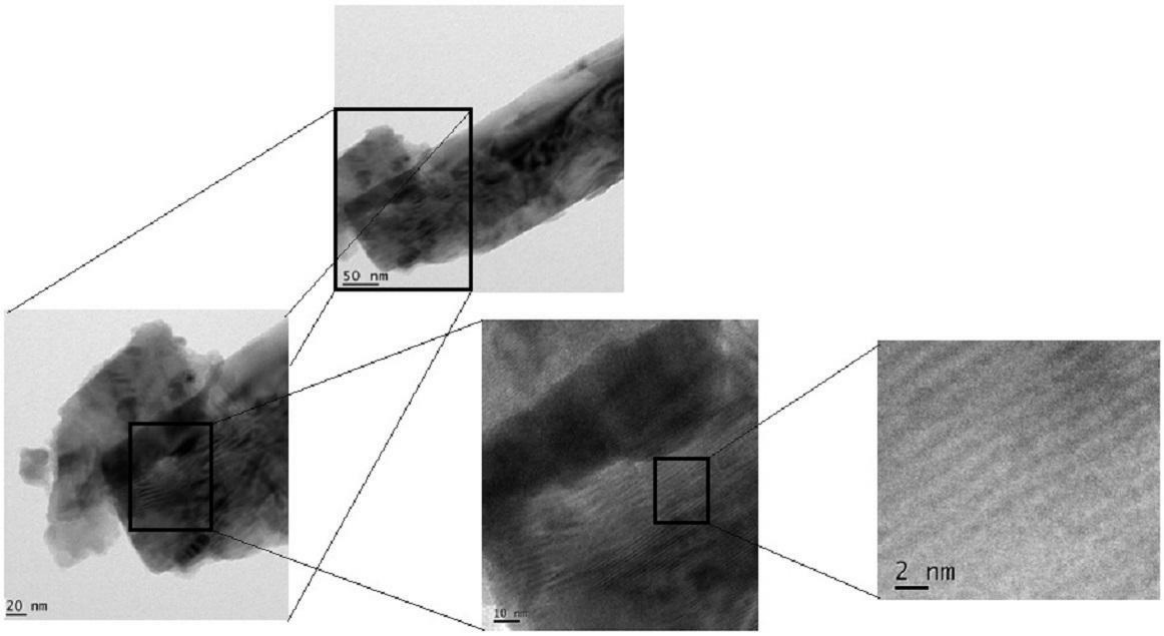

Fig. 3: TEM images of Sb_2Se_3 rod showing steps and kinks.

Chemical and structural analysis

Purity, homogeneity and phase stability are the paramount factors desirable for the preparation of compounds with suitable device characteristics, as non-stoichiometry influences their physical properties. A binary compound is assumed to be stoichiometric when the atomic constituents present in the ratio 1:1, 1:2, 2:3, 3:7 etc. (Ajayakumar & Kunjomana, 2016). In this regard, the chemical characterization of synthesized samples is inevitable for detecting the existence of undesirable components, homogeneity, microstructure, and crystalline phase. Therefore, the as-grown spheres were subjected to EDAX and XPS analyses. The recorded energy dispersive analysis spectrum (Fig. 4a) allows to compute the composition of Sb and Se as 39.95 and 60.05 at.%, respectively, which is in agreement with the ideal stoichiometry, 2:3 (at.% = 40:60). Peaks due to oxygen were not found around 1 keV, which justifies that the spheres are free from oxygen contamination. In the present work, as the nanocrystals were kinetically driven by optimizing the supersaturation under high vacuum in the absence of extraneous raw materials and gaseous catalytic agents, the right chemical proportion of antimony and selenium was identified, devoid of other elements. On the other hand, Wang et al. (2011) analyzed the Sb:Se

atomic ratio as 37.2:62.8 in Sb_2Se_3 products, where the lack of stoichiometric composition exists due to the synergetic effects of process parameters such as temperature, heating mode, and precursor concentration. The reported results show that there is a good control of composition in the PVD grown spheres, which were developed facile without any complicated chemical reaction or modulated by precursor concentration. The elemental maps (Fig. 4(b-c)) generated based on the EDAX profile (Fig. 4(a)) further confirm the stoichiometric formation of Sb_2Se_3, showing that Sb and Se are evenly distributed in the lattice.

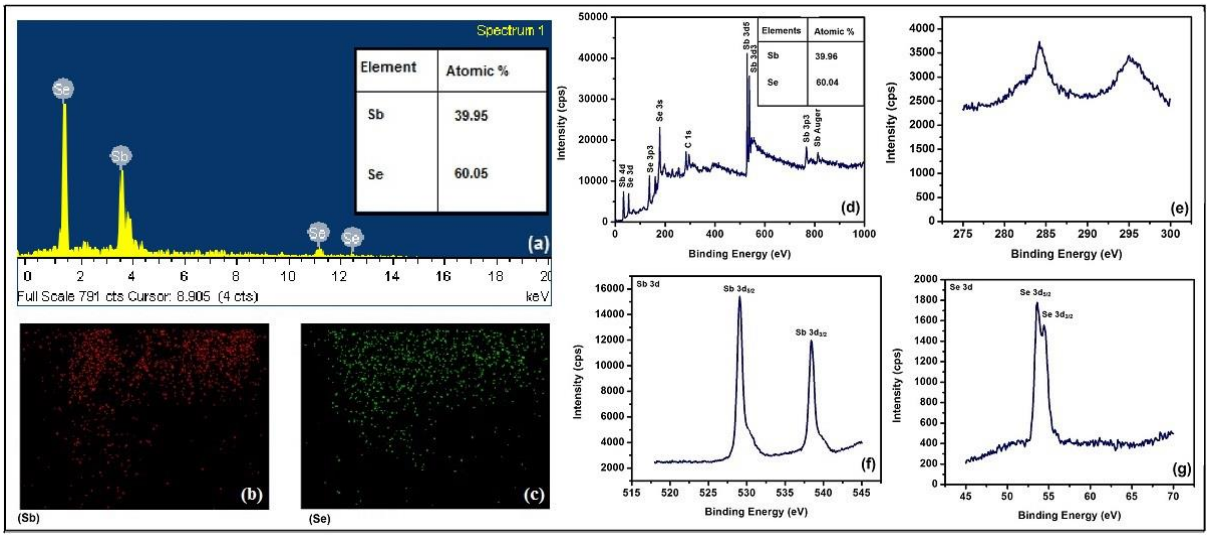

Fig. 4: (a-c)EDAX spectrum and elemental maps of Sb, Se showing the presence of constituent elements in the as-grown spheres; (d) XPS wide range spectrum of Sb_2Se_3; (e) Core-level spectra of carbon and the vicinity of (f) Sb 3d and (g) Se 3d bands.

The surface chemistry of the PVD grown Sb_2Se_3 spheres based on composition and valence states were further probed in detail by X-ray photoelectron spectroscopy using monochromatic Al Kα (1486 eV) excitation (Kratos AXIS Ultra DLD). Figure 4d represents the XPS survey spectrum of spheres and the inset shows the ratio of Sb:Se as 39.96:60.04 at.%, which is fairly in accordance with the recorded EDAX data. Thus, the aforementioned analyses justified the right proportion of the host component elements. The binding energies corresponding to the Sb 3d and Se 3d core levels were found to be consistent with that reported in the literature (Wang et al., 2011 &Liu et al., 2014). Figure 4f shows the magnified spectrum

of antimony selenide in the vicinity of Sb. Doublet peaks from Se $3d_{5/2}$ and Se $3d_{3/2}$ subshells emerged due to spin-orbit coupling as displayed in Fig. 4g. The binding energy values are given in Table 3, which are comparable to that reported by Mehta *et al.* (2010).

Table 3: Binding energies for Sb $3d_{5/2}$,Sb $3d_{3/2}$ and Se $3d_{5/2}$ and Se $3d_{3/2}$

Levels	Sb $3d_{5/2}$	Sb $3d_{3/2}$	Se $3d_{5/2}$	Se $3d_{3/2}$
Binding energy (eV)	529.1	538.4	53.6	54.4

Wang et al. (2011) reported the presence of oxygen 'O' 1s corresponding to the binding energy, 529.2 eV, in Sb_2Se_3 wires prepared by gas-induced reduction route method. Liu et al. (2014) detected the presence of Sb_2O peak in Sb_2Se_3 thin film surface fabricated by employing thermal evaporation method. The authors etched the samples by Ar^+ iron at 600 s (~10 nm thickness) to remove the traces of oxygen but failed to detect pure Se from the measurement. Wang et al. (2016) cleaned the electrodes by rinsing with propylene carbonate to remove superficial impurities for XPS analysis, whereas in the present work, prior care was taken to avoid such kind of oxygen contamination by employing high vacuum without any post treatment and from XPS, it was possible to detect the presence of antimony and selenium elements in tune with the composition of Sb_2Se_3.

X-ray diffraction studies are critical for providing evidence to identify the crystal structure, unit cell parameters and phase of the grown crystals. The PXRD profile of the physical vapor deposited Sb_2Se_3spheres is depicted in Fig. 5a, which confirmed orthorhombic symmetry with lattice parameters (a = 11.62 Å, b = 11.79 Å and c = 3.97 Å) in agreement with the JCPDS 15-0861data. Diffraction peaks corresponding to any other phases were not found. The characteristics of sharp and strong peaks indicate appreciable crystallinity of the harvested product. The narrow peak width and shape refer to the low lattice distortion of the vapor grown crystals. Moreover, increment in the intensity of peaks from the planes (130), (230), (211), (221) and (250) was identified due to the improvement in atomic periodicity than that of chemically synthesized ultra-long Sb_2Se_3 nanostructures by Yu et al. (2006). The X-ray diffraction data thus validates the stoichiometric yield of antimony selenide samples, devoid of other phases or

impurity elements.

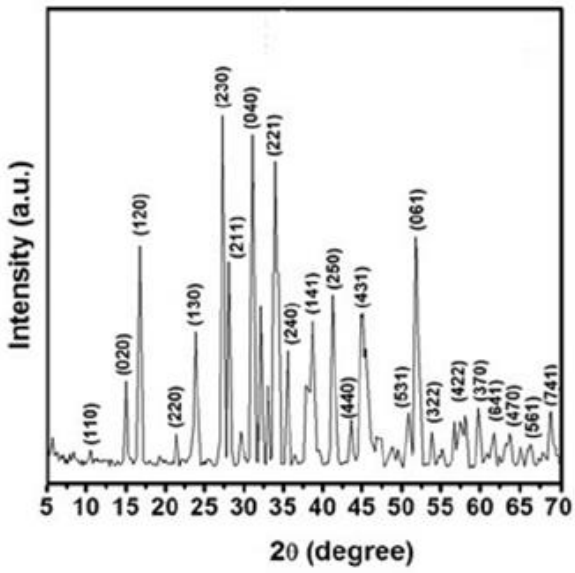

Fig. 5: X-ray diffractogram of Sb_2Se_3 spheres recorded for the angle 2θ between 5°-70°.

Optical properties of the vapor grown habits

UV-Vis-NIR and photoluminescence spectra aid in the analysis of energy gap and nature of transition. The optical absorption data of the as-grown habits were recorded in the wavelength range, 200-2000 nm. The absorption coefficient (α) varies with the incident photon energy ($h\nu$) as per the Tauc relation,

$$(\alpha h\nu)^2 = A\,(h\nu - E_g) \qquad (3)$$

where A is a constant and E_g is the energy band gap. The plot of $(\alpha h\nu)^2$ versus ($h\nu$) characteristics enabled to evaluate the band gap energy (Fig. 6a-b). In the present work, the PVD grown antimony selenide crystals exhibited direct allowed transition. The energy gap values of microfibers, rods, octahedra, and spheres are found to be 1.25, 1.47, 1.51, and 1.75 eV respectively (Fig. 6a-b). But, the optical absorption experiments conducted by Yu et al. (2006) showed lesser band gap (1.15 eV) for the Sb_2Se_3 samples prepared by chemical route. Chang et al. (2007) computed the energy gap of antimony selenide forms grown by Solvothermal process

as equal to 1.49 eV. Vadapoo et al.(2011) reviewed the values of the band gap (1.13-1.49 eV) for Sb_2Se_3 nanostructures grown by various chemical methods.

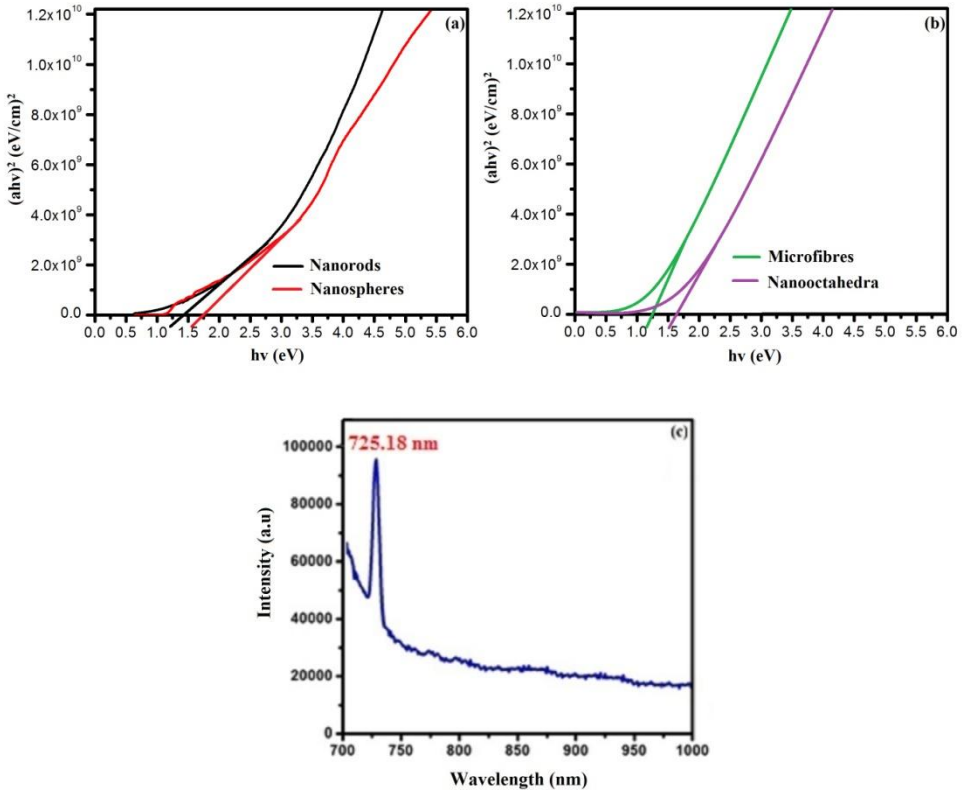

Fig. 6: Plots of $(\alpha hv)^2$ versus photon energy: (a) rods and spheres; (b) fibres and octahedra and (c) PL spectrum of spheres.

Table 4 lists the extrapolated energy gap values of as-grown Sb_2Se_3 micro and nanoforms, which are found to be larger than that prepared by other researchers using microwave-activated solvothermal reactions, vapor-liquid-solid technique and hydrothermal synthesis process (Mehta et al., 2010; Yang et al., 2015; Yu et al., 2006 & Chang et al., 2007). In the case of former, increase in band gap is attributed to good crystallinity, improved stoichiometry, large surface to volume ratio and quantum confinement of the nanoparticles compared to bulk materials. The experimentally obtained results are thus optimum for solar energy conversion, implying that Sb_2Se_3 nanocrystals of tunable band gap endow enormous applications in photovoltaics.

Table 4: Optical band gap of PVD grown Sb_2Se_3 crystals

Sb_2Se_3 crystals	Direct band gap (eV)
Fibers	1.25
Rods	1.47
Octahedra	1.51
Spheres	1.75

The photoluminescence spectrum (PL) is an indispensable surface sensitive tool to investigate the emission band structure, presence of defects and the optical parameters of a semiconductor. However, the band gap of PVD grown Sb_2Se_3 spheres was not elucidated by earlier researchers. Figure 6c shows the photoluminescence spectrum of Sb_2Se_3 spheres which were recorded at room temperature by subjecting to an excitation wavelength of 700 nm. The emission spectrum showed a sharp and intense peak at 725.18 nm. Predominantly, the near band gap luminescence has exhibited donor-bound excitation transition, free excitation transition, and a donor to valence band transition. The PL studies of hydrothermally grown antimony selenide nanostructures were carried out by Ota & Srivastava (2010) and a band gap equal to 1.71 eV was reported. These samples lacked crystallinity and the presence of impurity elements such as oxygen and carbon was evident from their EDAX spectrum. But, the vapor deposited Sb_2Se_3 samples are crystalline, stoichiometric and devoid of any foreign elements and hence exhibited good optical characteristics in agreement with UV-Vis-NIR data.

Material engineering

The quality of a binary semiconducting crystal, which depends on long range atomic arrangement and composition, governs desired properties and therefore, it is essential to control the synthesis protocols for device applications. In this regard, physically unique and chemically uniform Sb_2Se_3 compound was initially prepared by filling stoichiometric proportions of high pure (99.999 %) elements, Sb and Se (procured from Nuclear Fuel Complex, India) into an ultrasonically cleaned quartz container (1 cm bore size and 10 cm length). The high vacuum ($\sim 10^{-6}$ mbar) sealed ampoule comprising the constituents was packed using ceramic wools, placed in a muffle furnace and stabilized at 720 °C with the aid of a temperature controller (TC). It was regularly rocked at a rate of 60 rpm, utilizing a dynaflux synchronous motor coupled to

the ceramic tube (Fig. 7).

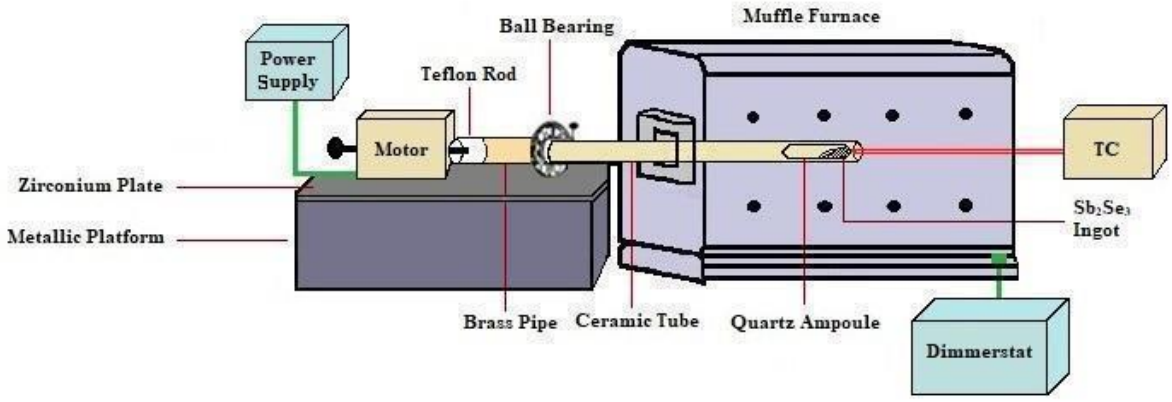

Fig. 7**:** Schematic of constant temperature furnace coupled with rotation mechanism

After slowly cooling to ambient temperature, ingot was formed with the right composition (39.99:60.01) close to the standard atomic ratio (40:60) of the compound, devoid of foreign substances, structural irregularities and defects. This solidified charge obtained under the optimized experimental conditions was powdered, filled in another ampoule (20 cm length and 1.5 cm diameter), closed under very low pressure and subjected to reverse transport by setting the growth zone at a higher temperature than the melting point, 611 °C, for cleaning at the finest level. A cost-effective approach was further applied to obtain crystals by inserting the sealed quartz tube containing the stoichiometric constituents in an indigenously assembled horizontal gradient furnace with relay-controlled mechanism, adopting the principle of PVD process. Systematic experimental trials were carried out for the bulk crystallization by promoting mass transport of vapors. The driving force has been facilitated in terms of supersaturation governed by $\Delta T = T_N - T_G$, where T_N and T_G are the thermodynamic extrinsic variables utilized for accomplishing progressive phase transition to harvest Sb_2Se_3 solid crystalline habits.

Bulk vapor growth of Sb_2Se_3 crystals

Novelty of sublimation process lies in the modification of crystalline habits under a controlled environment, but the production of physically distinct crystals is at stake due to the difference in partial vapor pressures of the constituent elements of a binary system (Ghosh. 1993,

Sunagawa. 2007). Lack of uniformity in elemental proportion and presence of impurities are prone to induce trapping centres, which are detrimental to the photovoltaic performance. In this regard, Bibin and Kunjomana (2019) have described the growth mode of Sb_2Se_3 by limiting the mass transfer, from high to low concentration inside the ampoule based on the concepts of particle diffusion. But these samples were prepared by directly subliming the unprocessed raw Sb_2Se_3 compound, which was not subjected for melt mixing and thus were susceptible to off-stoichiometry as revealed from the EDAX analysis (39.95:60.05) and resulted in agglomerates. In order to prevent this complexity, first and foremost, the stoichiometric precursor of antimony selenide was engineered using a muffle furnace (Fig. 7) as described by Reshmiet al. (2011). For this purpose, the synthesis procedure was carried out by adopting solid state reactions of the reagents, Sb and Se (Fig. 8a) at 720 ℃. Slow cooling was facilitated to attain thermodynamic equilibrium, so as to process the chemically homogeneous Sb_2Se_3 ingot as shown in Fig. 8b.

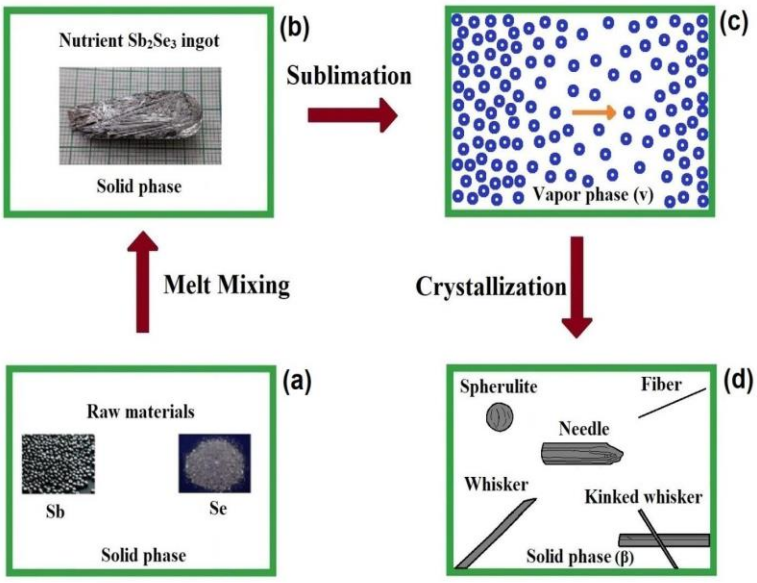

Fig. 8: Physical processing route comprising melt mixing of raw materials leading to the formation of stoichiometric ingot, sublimation of atoms (marked as blue circles); orange colored indicator point the direction of vapor flow towards substrate and crystallization of different habits

The powdered form of this ingot sealed in the quartz ampoule, devoid of any catalyst, was vaporized and allowed for physical vapor deposition in a customized furnace (Fig. 9) in order to explore the relationship between internal microstructure and physical properties. The temperature of nutrient and substrate zones, T_N and T_G, was held constant independently using programmable controllers. Prior to the PVD process, reverse transport has been intentionally applied such that the crystallization region was stabilized at high temperature (720 °C) which enabled the removal of tiniest or minute particles. Subsequently, crystallization was carried out by adopting a bottom-up approach to enhance the addition of atoms (Fig. 8c) on the cleaned growth region, and thus the system has undergone transition from non-equilibrium to equilibrium for the development of characteristic morphologies (Fig. 8d).

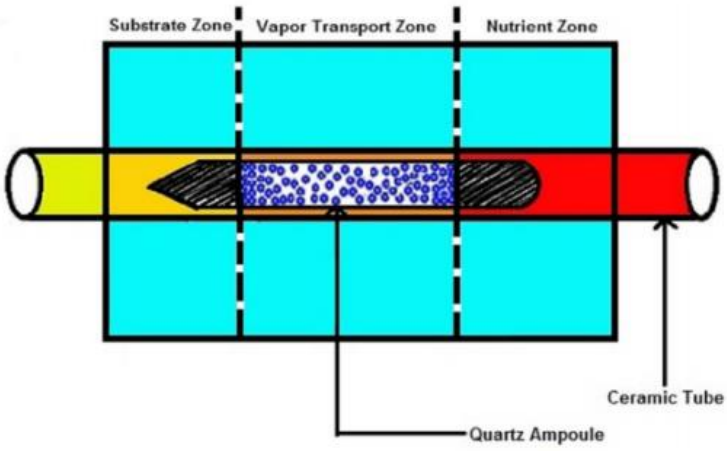

Fig. 9: Schematic model showing the three regimes: nutrient, vapor transport and substrate zones in the growth chamber (Bibin and Kunjomana, 2019)

Thus the customization of stoichiometric Sb_2Se_3 ingot followed by physical vapor deposition was fair enough to yield chemically homogeneous crystalline habits such as fibers, whiskers, needles and spherulites. Since these forms are governed by the particle diffusion due to mass flow, internal structure and experimental conditions, etc., the PVD process was systematically carried out under different stabilized synthesis conditions as presented in Table 5.

Table 5: Effect of extrinsic variables on morphology, lattice parameters, density and band gap of Sb_2Se_3 crystals

T_N (°C)	T_G (°C)	T_N-T_G (°C)	Crystalline habits	*A* (Å)	*b* (Å)	*c* (Å)	Density (g/cm^3)	Band gap (eV)
685	560	125	Coir-like fibers (Fig. 4)	11.6328	11.7798	3.9846	5.8437	1.17
710	530	180	Whiskers (Fig. 5a)	11.6331	11.7801	3.9849	5.8429	1.15
760	530	230	Needles (Fig. 9)	11.6327	11.7797	3.9844	5.8441	1.16
880	530	350	Spherulites (Fig. 10)	11.6325	11.7794	3.9840	5.8449	1.18

The degree of supersaturation was optimized in terms of difference in temperature, since the driving force, *S* is directly dependent on ΔT (Reshmi et al. 2011). The formation of filamentary type crystals is influenced by the mode of heterogeneous nucleation and successive growth process. Though different fiber-like morphologies were detected in various alloys, composites, polymers, etc. such habits were rarely reported in physically deposited chalcogenides (Qi et al. 2001, Jabbouret al. 2012, Manivannan et al. 2020). Coir-like fibers (Fig. 10) were deposited when ΔT was stabilized at 125 °C so as to increase the mass transport than that subjected earlier for yielding low dimensional habits (ΔT = 60 to 90 °C) by the authors (Bibin and Kunjomana, 2019). The average length (~3.25 mm) and width (~10-20 μm) of the former habits were estimated using *Image J* software. Arrays of fiber-like whiskers have also been observed by Wang et al. (2003) in a crossed network synthesized from hydrothermal process using chemical precursors, but exhibited oxidized selenium species. But the PVD grown Sb_2Se_3 fibers were devoid of such foreign elements. Moreover, these stoichiometric samples were grown in straight line geometry and could be singled out unlike the spherical, octahedral and rod shaped tiny crystalline deposited under low supersaturation (Bibin and Kunjomana, 2019). Coir-like fibres are slender (Fig. 10a) as a result of the fast incorporation of atoms from the mother phase (v) along the radial *c*-axis. As per the theory of crystal growth, favorable atomic attachments on the growth zone are governed by the exothermic process of crystallization with the release of enthalpy (ΔH) following the thermodynamic relation, $\Delta G = \Delta H - T_G\Delta S$, where ΔG is the change in Gibbs free energy and ΔS, the difference in entropy between the two

phases, ($S_\beta - S_V$) (Arnberg et al. 2012). But in the present work, tiny crystalline deposits in the form of flakes were detected as shown in Fig. 10a on the crystal surface, because of the anisotropy in ΔG during growth at T_G = 560 °C, deteriorating the quality of fibers. The same location as in Fig. 10b is depicted inside the yellow ringed outline within Fig. 10a, exhibiting the flakes and the fibers of the enlarged exterior structure in detail. The dimensions of crystals were increased so as to obtain thick fibers, owing to the boost in vapor transport corresponding to T_N = 695 °C. Similar type of flattened over deposits were densely packed on these crystals grown at the same elevated growth temperature, as a result of the advancement of rough v-β interface associated with the disordered flow of thermal energy of the system and anomaly in latent heat of condensation during solidification. In order to accomplish atomically smooth interface and eliminate defective structures, an attempt was done by intentionally reducing T_G to 530 °C.As a result, whiskers of length (l), 155 μm and width (w), 45 μm with the ratio, $R = l/w$ equal to 3.44, were obtained after slow cooling. Zhigadlo et al. (2013) have discussed that, if $R > 1$, crystals presume the shape of whiskers. The direct superior approach over our previous research work [28] by enhancing T_N to 710 °C and decreasing T_G to 530 °C (Table. 5) enabled mass transfer for bulk crystallization, attenuating imperfections, as flat faces were developed with sharp tip as shown in the Fig. 5a-b.

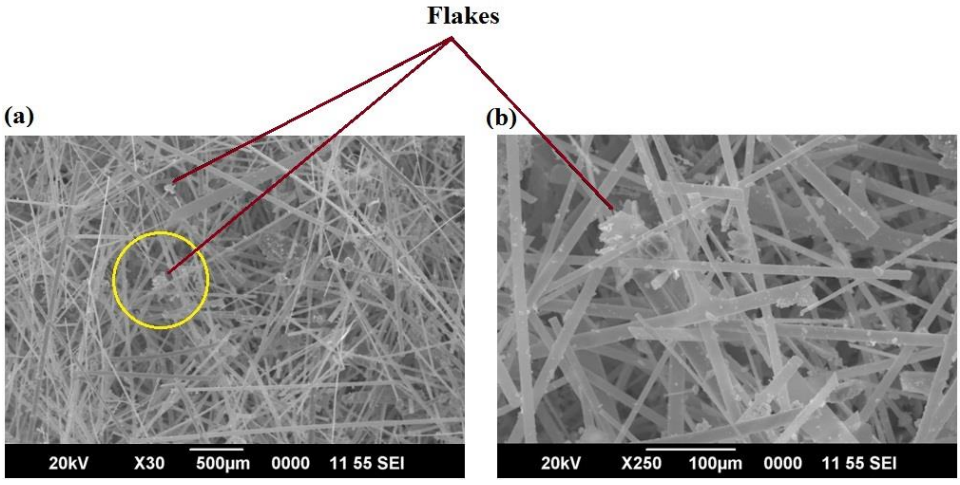

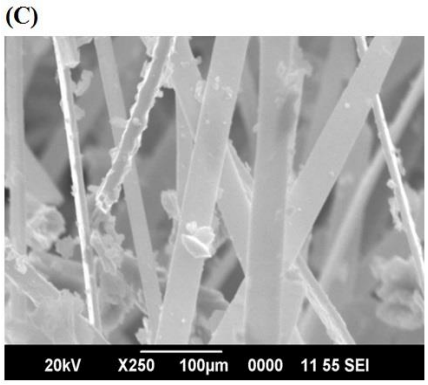

Fig. 10: SEM images of (a-b) thin coir-like fibers and (c) thick coir-like fibers

The unidirectional crystallization of whiskers has been promoted by the incorporation of ad-atoms on a stable nucleus owing to the progression of smooth planar vapor-solid interface initiated under optimized supersaturation. The Gibbs free energy becomes minimum due to the ordered close packed atomic arrangement along the side faces and thus lateral spread gets attenuated (Brenner, 1958). These whiskers attained equilibrium configuration with the evolution of low energy side faces and further growth was initiated on the tip (Fig. 11b), which is related to the inherent orthorhombic system. As per the report of Sunagawa (2006), crystal species with size, $a \approx b > c$ have the ease to grow in the form of prismatic elongated habits, which could reflect in the Sb_2Se_3 whiskers, since they grew with unit cells of dimensions, a = 11.6331 Å, b = 11.7801 Å and c = 3.9849 Å (Table. 5). Similar morphology was found on Sb_2S_3 chalcogenides bearing orthorhombic crystal system, synthesized by microwave-assisted solution-phase approach (Wang et al. 2003). Smith et al. (1979) reasoned the rapid whisker development in terms of multiple nucleation due to very large transport of nutrients and hence observed spirals on the surface. Further advancement of layers gave rise to a fairly uniform surface as presented in Fig. 11a. In the present research work, the synthesis of filamentary shaped antimony selenide followed the theory of nearly perfect form of solid state based on the Kossel, Stranski and Volmer (KSV) model (Brenner, 1958), as the crystals did not exhibit any helical or twisted structures associated with spiral dislocation mechanism.

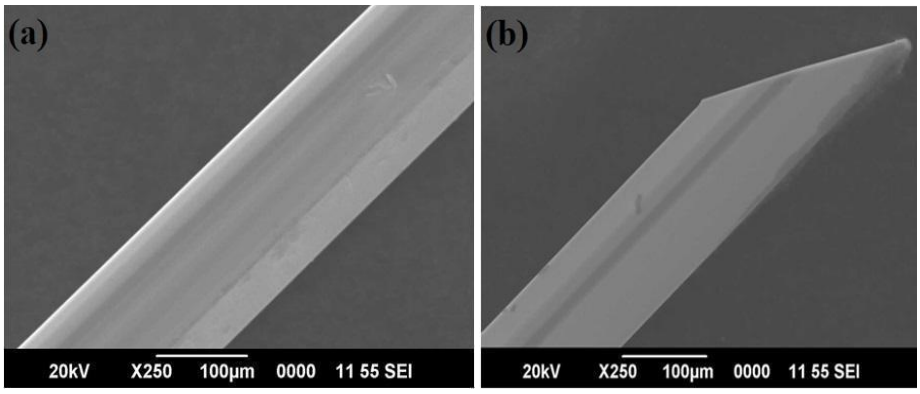

Fig. 11: SEM images of whiskers (a) smooth face (b) sharp tip

Based on this atomic theory, a vicinal or incomplete surface comprises a flat layer partially covered by another one (Fig. 12), such that the boundary line where there is a difference of level equal to an intermolecular spacing between its two sides is called a step (Varma, 1953). The growth of a crystal depends on the transport of vapors in the deposited region, diffusion of ad-atoms and attachment to the kinks on the surface (Fig. 12). Two processes are likely to occur during crystallization such that some of these atoms leave the substrate, while others arrive from the nutrient zone.

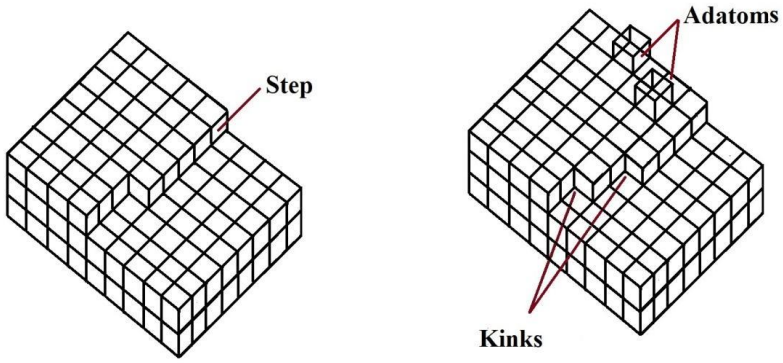

Fig. 12: Schematic of vicinal surfaces depicting growth steps, kinks and adatoms

If supersaturation is increased, more adatoms from the vapor diffuse over the growth sites, give up their kinetic energy and are probable to get settled on the kinks as depicted in Fig. 12. As a result of successive tangential deposition of atoms, the layers were stacked on the

surface as shown in Fig. 13a, and it resembles the microscopic images of Wu et al. (2015) on Sb_2Se_3 whiskers. During the development of crystalline habits, there are chances of perturbations in thermal stability and in this case whiskers with over deposition of small spurs on the edge appeared as shown in Fig. 13b. Similar features were detected by Martins et al. (2011) on tubular organic crystals. However, there are no indications of screw dislocations in the PVD grown Sb_2Se_3 samples. Mass transfer thus plays a vital role in moulding the shape of samples during crystallization.

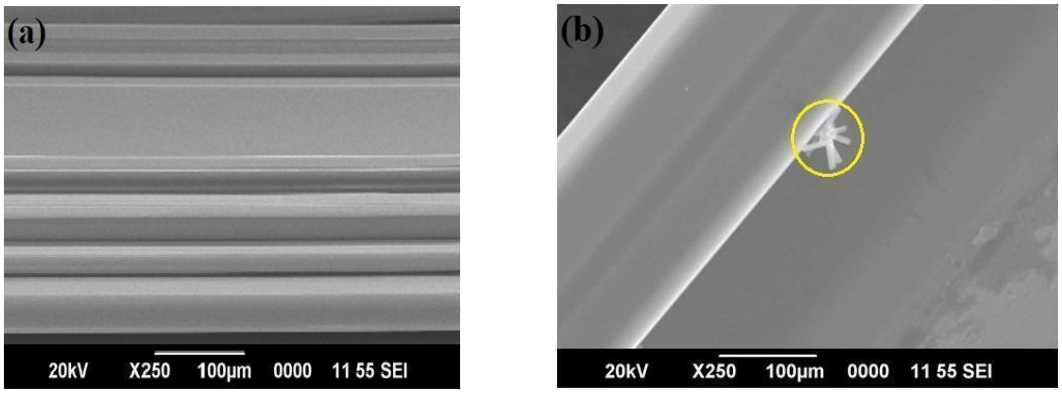

Fig. 13: SEM images of crystal surfaces showing (a) parallel growth steps (b) deposits of spurs on the whisker

Partially developed specimens with hollow topography (Fig. 14a) were also found in the inner walls of the ampoule, attributed to the lack of material supply, in agreement with the research findings on Se-Te whiskers grown from vapor phase (Trivedi. 1976). Figure 14b displays the merging of two crystals which are misaligned, resulting voids in between them. The space filling within the channels by condensation of atoms gave rise to the progression of layers on the surface owing to the advancement of growth steps towards the tip (Fig. 14c). The thermal fluctuations associated with vaporization and subsequent condensation processes promoted anisotropy in the driving force and hence induced overgrowth of whiskers (Fig. 14d).

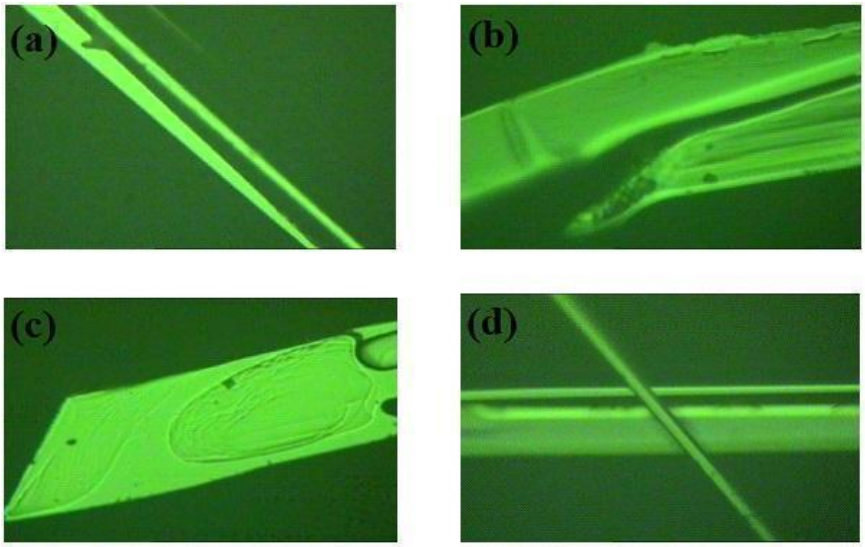

Fig. 14: Optical micrographs of (a) hollow whisker (b) conjoined whisker (c) propagation of layers and (d) combined whiskers (350×)

Enhancement in the driving force for mass transfer and elevating the concentration gradient by increasing T_N to 760 °C, retaining the same T_G (530 °C) could yield thick needle habits with growth steps (marked in yellow colour, Fig. 15a) as detected for whiskers, following the KSV mechanism. Higher supersaturation persuaded a rough interface and so upon enhancing ΔT from 230 °C to 250 °C (T_N = 780 °C &T_G = 530 °C), though the surface became fairly smooth in some regions as depicted in Fig. 15b, they have grown amid defective structures.

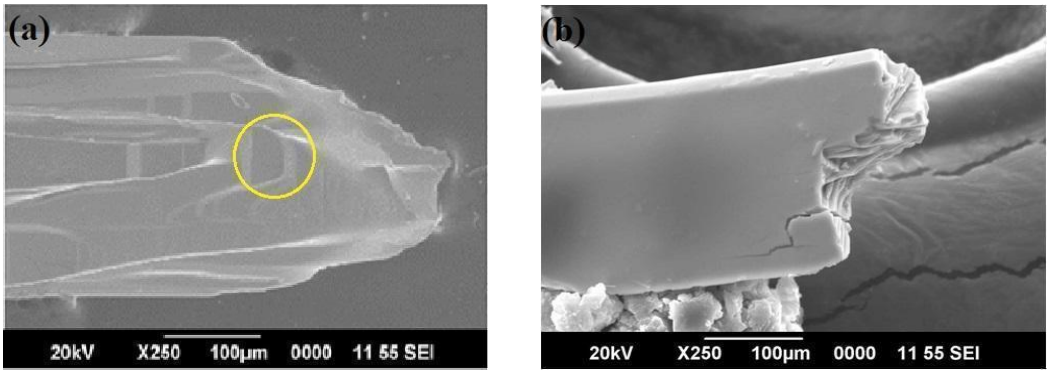

Fig. 15: SEM images of needles (a) growth steps and (b) polycrystals

On the other hand, spherulitic crystals of antimony selenide could be produced (Fig. 16a)

analogous to $NaHCO_3$ and In_2Te_3 (Sangwal, 2007) with further intensification of T_N to 880 °C. Figure 16b shows the pile up of striations and hillocks on an irregular surface of a typical spherulite. In the present work, due to the progression of diffused vapor-solid interface, the surfaces of needle and spherical shaped samples (Fig. 15b and 16b) were developed with inferior quality due to the anomaly in deposition of atoms. Thus the above research findings could justify the fact that precise control on the nature of the interface during phase transition from v to β is mandatory, because it influences the microstructures and physical properties.

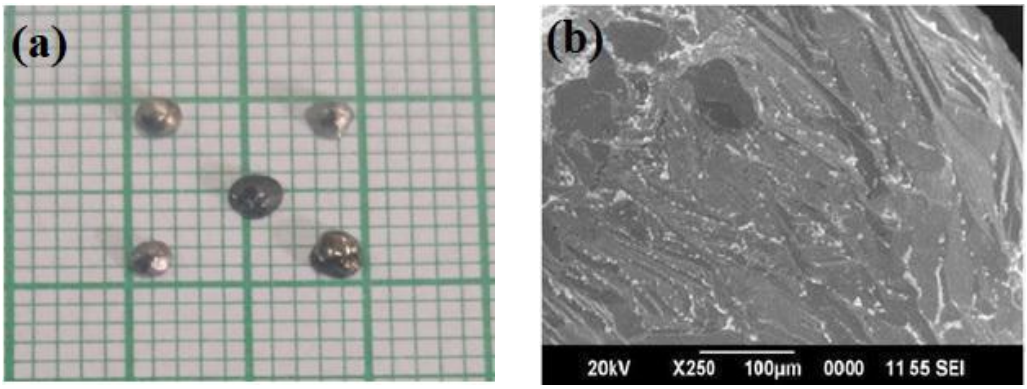

Fig. 16: Photographs of (a) spherulites (1 division = 1 mm) and (b) fibrillar structure on the rough surface

Physical properties of Sb_2Se_3 crystalline habits

The properties of bulk crystals are greatly influenced by lattice disorders, compositional variations, presence of foreign matter, change in morphology, etc. Therefore, the diverse habits obtained during vapor growth have been examined using a powder X-ray diffractometer, since PXRD is the best suited fingerprint technique for structural and phase identification. Figure 17 depicts allowed reflections corresponding to the orthorhombic system of antimony selenide, which aligns with the results of Tideswell et al. (1957). The indexing of peaks did not show systematic absences of reflections for (hkl) or (hk0), yet extinctions were detected in (h0l) for h+l odd, and (0kl) for k odd. Diffraction from the planes, thus obeyed above conditions with proper matching of intensities, which implies that the grown Sb_2Se_3 layered samples belong to the Hofmann's space group, *Pbnm.* In all the profiles (Fig. 17), the intensity of the diffracted X-

ray beam is highest for the peak from the (221) plane positioned at $2\theta = 31.16^{o}$. However, in the present work, the diffractograms showed a lesser number of peaks indicating high degree of crystallinity unlike that reported on the products synthesized by hydrothermal and microwave assisted methods using mixtures of chemical reagents (Wang et al. 2003). It is vivid that the strongest reflections caused by the mutual reinforcement of scattered radiations accord to the standard JCPDS Card No: 15-0861, since the stoichiometric Sb_2Se_3 ingot was employed for sublimation process under high vacuum, justifying the periodic arrangement of crystallites. Ghosh (1993) discussed the mass spectroscopic study of laser induced vaporization of Sb_2Se_3 comprising a complex mixture of Sb_4, Sb_2Se_2, SbSe and Sb_2 species, which were not found in the present crystals as they grew in chemically homogeneous elemental proportion. The merit of PXRD is thus utilized to disclose single phase Sb_2Se_3 with the right composition, which enabled the optimization of T_N and T_G so as to yield good quality crystals.

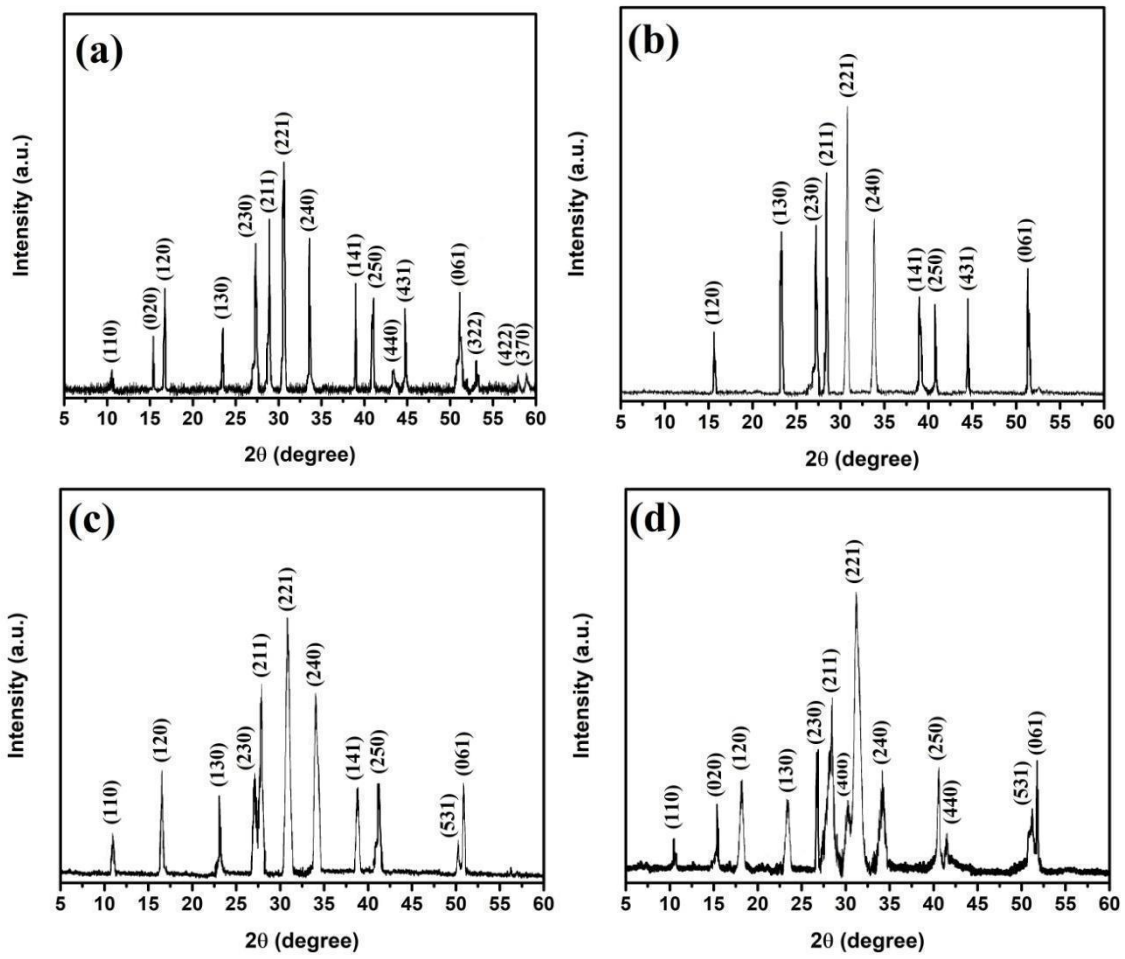

Fig. 17: Powder X-ray diffraction patterns of (a) coir-like fibers (b) whiskers (c) needles and (d) spherulites

Figure 11a shows the PXRD profile of Sb_2Se_3 fibers with reduced number of diffraction lines, devoid of humps than that reported in the literature (Bibin and Kunjomana, 2019), indicating appreciable degree of crystallinity. These samples exhibited sharp peaks from the planes reflecting the characteristics of nearly perfect crystals unlike those grown from melt, chemical vapor transport and hydrothermal routes (Tideswell et al. 1957, Wang et al. 2003). However, the cell dimensions of fibers (Table. 5) are slightly deviated from the standard JCPDS card data, because of the presence of over-deposits on the surfaces. Optimization of growth temperature by stabilizing 530 °C, facilitated the development of good quality whiskers with the prominent existence of main maximum (Fig. 17b) over all the subsidiary maxima as a result of coherence in the scattered beams due to electrons localized with proper lattice alignment. Number of diffraction peaks are found to be less, but strong compared to that observed for the fibers due to the enhancement of periodicity with the progressive advancement of smooth interface and the precise control of microstructural development by very slow cooling. The values of lattice parameters, cell volume and density of as-grown whiskers are in accordance with the published work (Tideswell et al. 1957), justifying the formation of monophase antimony selenide. Upon augmenting mass transfer establishing higher ΔT (= 230 °C), inferior structural characteristics (Fig.17c) was found for needle shaped crystals than that of the whiskers, as the former grew owing to the onset of rough interface. The correlation between morphology and structure was further explored by increasing the nutrient zone temperature to 860 °C, which disrupted the degree of crystallinity as a few humps emerged in the diffractogram of spherulites (Fig. 17d). The PXRD patterns of the vapor grown samples were refined by Rietveld analysis whole-pattern fitting based upon the Full Proof software to accomplish the phase identification and as depicted in Fig. 18a-d (Shan et al. 2021). The results reveal that high purity of crystalline phases (monophase) and all the crystals were crystallized in an orthorhombic unit cell pattern with the *Pbnm* space group symmetry. Also the observed crystallographic data shows good consistency with the standard JCPDS Card No: 15-0861. On the other hand, the chemical vapor deposited antimony selenide rod-like structures using a precursor of $MeSb(Se^nBu)_2$ exhibited a large variation in the intensity of the powder X-ray diffractograms due to a restricted degree of

preferred orientation as reported by Benjamin et al. (2015). As whisker morphology is found to be superior in structural characteristics, it is subjected for EDAX and XPS analysis so as to probe the chemical composition. However, the present research findings validate the superiority of physically deposited crystals as they are free of foreign elemental contamination compared to other melt grown and chemically transported samples (Bacewicz and Ciszek, 1991, Wang. 2003).

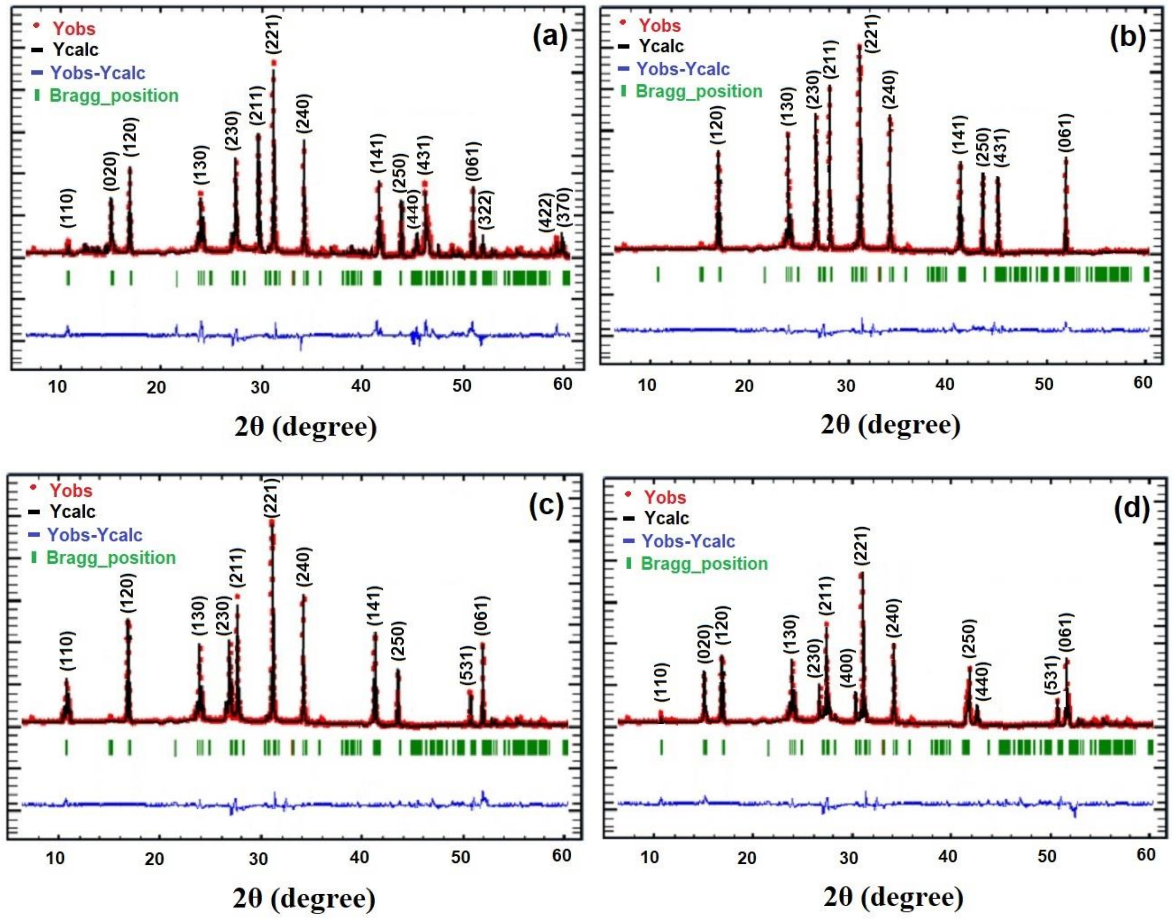

Fig. 18: Rietveld refinement patterns of (a) coir-like fibers (b) whiskers (c) needles and (d) spherulites

Growth of good quality crystals under optimized conditions improvises their optoelectronic parameters. Hence, in the present work, special attention has been given to elucidate the optical characteristics of harvested Sb_2Se_3 products based on UV-Vis-NIR and PL

studies. The band gap, E_g, of all samples (Fig. 19a-b) was estimated by using the relation, $\alpha = B\left(\sqrt{h\upsilon - E_g}\right)/h\upsilon$; where the absorption coefficient, $\alpha = 2.303\, A/t$. It is well known that, $h\upsilon$ represents the energy of absorbed electromagnetic radiation, *t*, the thickness of the sample, *A*, the absorbance and *B*, a constant that does not depend on frequency (υ) (Wang et al. 2003). The Tauc plot between $h\upsilon$ and $(\alpha h\upsilon)^2$ validated direct allowed transition, which facilitates the possibility for the movement of electrons from the highest state of valence band to the bottom of the conduction region without any change in crystal momentum. As a result, effective absorption of solar radiations with generation of charge carriers enhances the energy conversion. On the other hand, semiconductors like crystalline silicon and GaP have lesser absorption coefficient (~ 10^4 and 10^3 cm^{-1}, respectively), since it requires additional energy with the aid of phonons through lattice vibrations of the atoms in the crystal in order to conserve energy owing to indirect transition, and thus inhibit their capability for photovoltaic applications (Oda. 2007). The E_g(1.17, 1.15, 1.16, and 1.18 eV) values were computed and shown in Table. 5 for the as-grown vapor deposited Sb_2Se_3samples and are lesser than those reported for the cleaved melt counterparts (1.20 eV) comprising multi-grains (Black et al. 1957). The former exhibited appreciable lattice periodicity as reflected from the PXRD findings (Fig. 17 and 18) and so the fundamental absorption edge was also shifted towards lower energy (Fig. 13a-b). Among all the habits, the nearly perfect crystalline whiskers exhibited E_g equal to 1.15 eV. This is due to the fact that prominent overlapping of electronic energy levels associated with strong chemical bonding widened the band regions. The electrons are strongly bound to the periodically aligned atoms as per the Kronig-Penney model (Pillai. 1994), forming a set of continuous bands separated by forbidden region. On the other hand, in our earlier published report, the obtained tiny samples under very low mass transfer possessed values of E_g in the range, 1.75-1.25 eV owing to morphological instability and the discreteness of energy levels related to quantum confinement . In the present work, the optical measurements of whiskers provided higher α (= 2.38×10^5 cm^{-1}) at 600 nm, which promises the enhancement of photon absorption. It is interesting to note that the chemical vapor deposited films are found to be poorly adhered to the substrate, with less densely packed large rod-shaped crystallites, leading to a film of low density and non-uniform thickness. Hence, reliable measurement of the optical or electrical properties is not possible, even though they reported a very low band gap (1.10 eV) as reported by Benjamin et al. (2015).

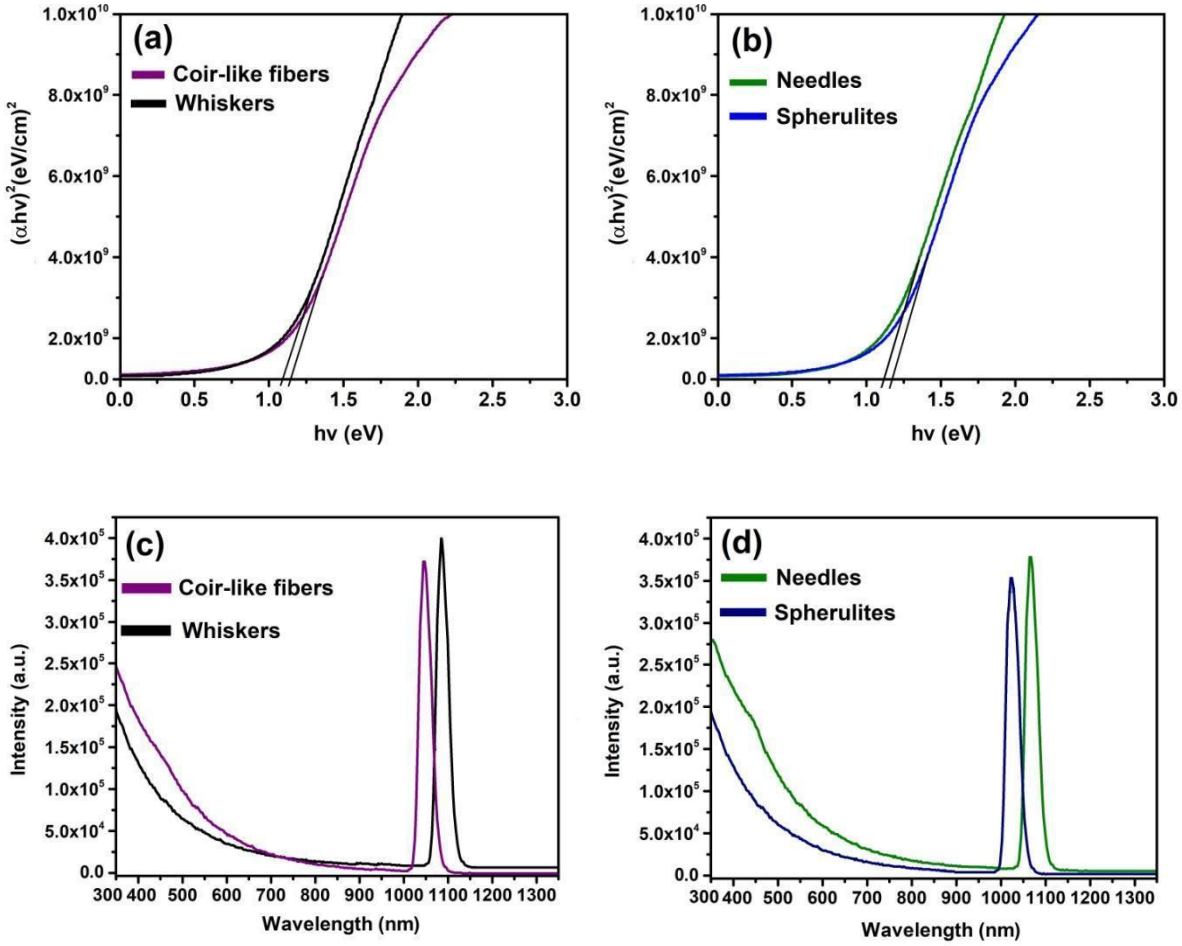

Fig. 19: (a-b) Plot of $(\alpha hv)^2$ versus photon energy and (c-d**)** photoluminescence profiles of the crystalline habits

The photoluminescence (PL) spectra (Fig. 19c-d) recorded at room temperature for the deposited antimony selenide crystals showed sharp peaks manifesting the band gaps, 1.18, 1.16, 1.17 and 1.19 eV and are comparable to those computed from the UV-Vis-NIR data (Table 1). Emission lines due to impurities like oxygen, nitrogen, etc. were not found, confirming the absence of foreign elements, since the samples were prepared using the customized stoichiometric Sb_2Se_3 precursor. Moreover, the synthesized habits exhibited intense peaks justifying the proper atomic arrangement as evident from the results of PXRD (Fig. 17 and 18). Among the morphologies, whiskers exhibited the most prominent peak at 1070 nm (Fig. 19c) corresponding to the energy gap, E_g = 1.16 eV, which point out enhanced generation of carrier

concentration. These crystals are devoid of defective structures due to the progression of smooth vapor-solid interface associated with optimum supersaturation and hence owned notable photoluminescence behavior, unlike coir-like fibers, needles and spherulites. As such, the whiskers were opted to explore their chemical, thermal, mechanical and electrical characteristics.

Chemical analysis

The phase purity of the prepared samples was examined with the aid of energy dispersive analysis by X-rays (EDAX). The customized charge after melt mixing revealed the right atomic proportion of elements (Sb:Se = 39.99:60.01 at.%) from Fig. 20a, confirming the formation of stoichiometric Sb_2Se_3 compound and so, it has been subjected for crystal growth as mentioned in the experimental section. Therefore, the deposited whiskers also possessed chemical homogeneity fairly close to that of the ingot (Fig 20b) comprising Sb:Se = 39.98: 60.02 at.% (Fig. 20b). Benjamin et al. (2015) have deposited Sb_2Se_3 rod-like crystallites by chemical vapor deposition using a complicated single precursor solution of $MeSb(Se^nBu)_2$. But, the EDAX survey shows a minor (1.46) variation in the Se/Sb ratio from the expected 1.50.

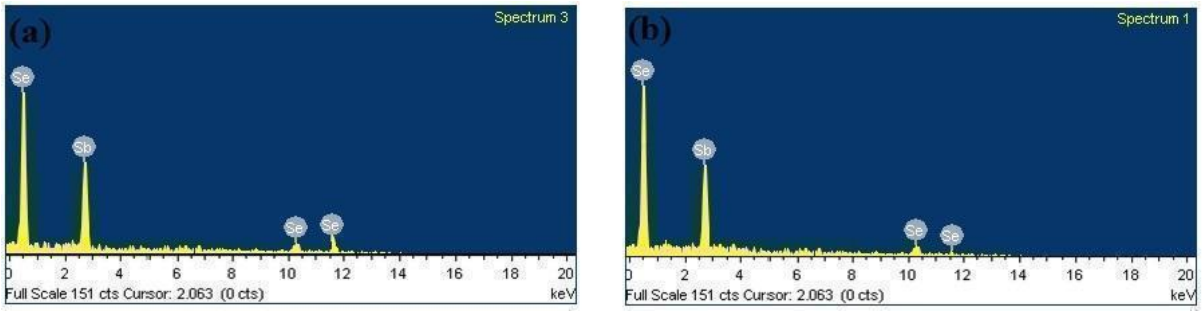

Fig. 20: EDAX spectra of chemically homogeneous Sb_2Se_3 (a) ingot and (b) whiskers

X-ray photoelectron spectroscopy (XPS) was also employed to provide information about composition of antimony selenide whiskers. Figure 21a represents the wide-range spectrum which enabled a comparable atomic ratio (39.97:60.03 at.%). Moreover, additional signals showing the presence of extraneous constituents were not observed from EDAX and XPS profiles and are consistent with the results obtained from PXRD, UV-Vis-NIR and PL

measurements (Fig. 17&18b, 19a and 20c), which validates the precise control of physical vapor deposition. The values of binding energies (BEs) were calibrated using the C 1s peak positioned at 284.6 eV (Fig. 21b) for the precise determination of BE as presented in Table. 6.

Table 6: Binding energies of antimony selenide crystals

Sb_2Se_3 whiskers	Binding energy (eV)			
	Sb $3d_{5/2}$	Sb $3d_{3/2}$	Se $3d_{5/2}$	Se $3d_{3/2}$
Vapor growth [Present work]	529.14	538.44	53.63	54.45
Hydrothermal growth (Liu et al. 2014)	529.00	539.40	53.60	--

Figure 21c-d depicts the high-resolution spectra in the vicinity of Sb 3d, and Se 3d, which exhibited peaks corresponding to Sb $3d_{3/2}$, Sb $3d_{5/2,}$ Se $3d_{3/2}$ and Se $3d_{5/2}$ sub-shells due to spin-orbit coupling and the surface electronic states of the samples have been identified. The chances of oxygen contamination could not be traced at the BEs, 530 and 60 eV respectively, which ruled out oxidation of the Sb_2Se_3 whiskers grown in the present work under high vacuum. On the other hand, for the same morphology prepared by hydrothermal process, the minor peak at 60 eV represents the oxidized Se species, like SeO_2 or SeO_3^{2-}. This is attributed to the addition of oxygen related organic solutions during the synthesis route (Wang et al. 2003), resulting in non-stoichiometry in their samples.

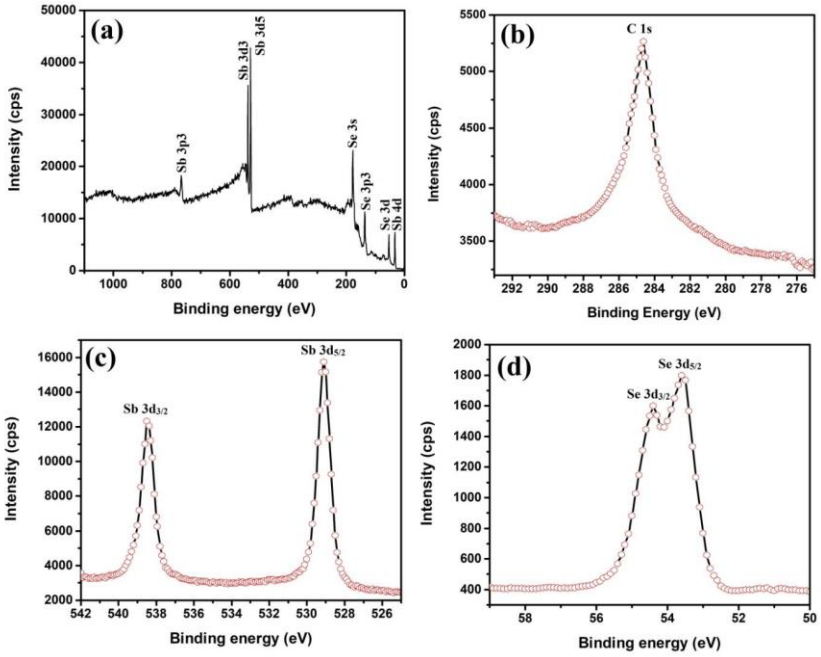

Fig. 21: (a) XPS survey spectrum and (b-d) core level spectra of vapor grown Sb_2Se_3 whiskers

In the present work, thermogravimetric analysis (TGA) revealed the right melting point (= 610 °C) for the grown samples bearing orthorhombic system, which justifies the absence of other phases, since there are no signs of additional peaks, as reported in the literature (Mavlonov et al. 2020, Tan. 2021). At very low temperatures, meagre weight loss is detected in the TGA curve (Fig. 16a), indicating the absence of moistures or oxygen attached to the crystal lattice and other organic or inorganic compounds (Yin et al. 2021). The 55 % weight loss of Sb_2Se_3 whiskers occurred between 600 to 615 °C, due to the thermal decomposition of the crystal at the melting temperature by weakening the bonds between Sb-Se. Leng (2008) has reported that the phase transformation occurs in the solids that have different equilibrium crystalline phases in various temperature ranges; such observations were not obtained in the TGA profile of the vapor deposited Sb_2Se_3 crystals. In general, glass transition occurs or is observed to be in the non-crystalline solid, which is referred to as the second order phase transition. It is distinguishable from first-order phase change in the crystalline solids. This research finding also validates with the present PXRD, EDAX and XPS analyses, because home-made stoichiometric Sb_2Se_3 charge was utilized for the deposition of antimony selenide crystalline habits. On the other hand, Liu et al. (2014) detected weight loss at 400 ºC due to the weak bonding of Sb and Se in their

synthesized Sb_2Se_3 powders.

The parameters such as hardness, yield strength, elastic stiffness constant and Young's modulus depend upon the type of binding force, internal arrangement of atoms in the lattice, deformation characteristics, etc. and were evaluated using the procedure as described by Teena et al. (2017). Mechanical properties are also highly sensitive to the quality of samples related to stoichiometry, which in turn is governed by precise control of the driving force during crystal growth. Therefore, the strength of as-grown Sb_2Se_3 whiskers bearing smooth surfaces were probed using a Vickers microhardness tester (Model: MVH-I). As reflected from the TGA profile, the strong covalent bonding between the constituent atoms was predominant so as to increase hardness up to 35 g, which further attained a maximum of 257.13 kg/mm^2 (Fig. 22b). After this load, slight decrease in the data has been observed till 100 g, owing to the minimal deformation occurred while performing indentation. Arivuoli et al. (1988) have reported that the vapor produced Sb_2Se_3 needles possess a significant number of grains/layered arrangements on the surface, which may be emerged due to the fast incorporation of atoms during the growth. Because of its polycrystallinity, this crystal exhibits extremely low hardness values (H_v< 40 kg/mm^2).

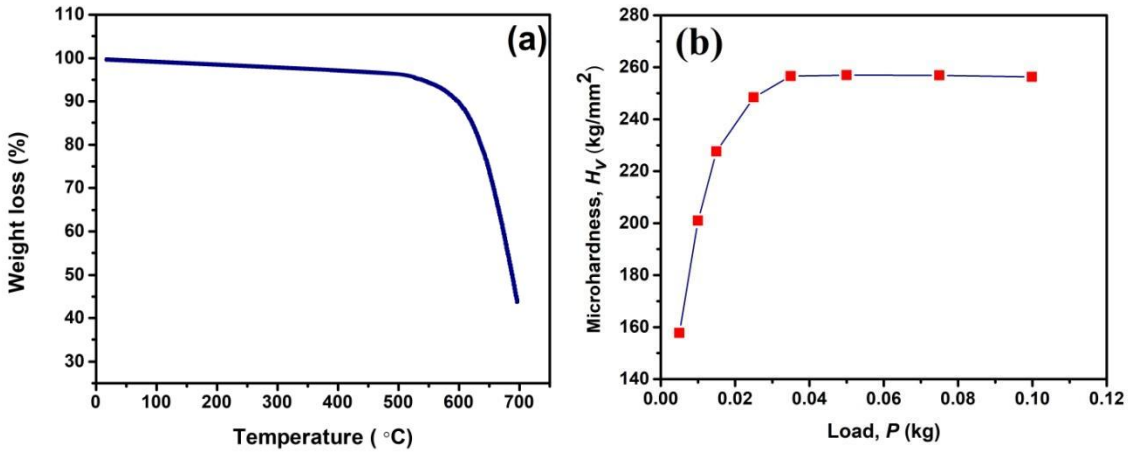

Fig. 22: Plots of (a) weight loss versus temperature and (b) microhardness versus load of Sb_2Se_3 whiskers

Furthermore, the saturation of hardness occurs because of the reciprocate interaction among the inherent defects in the real crystals with that of the additional extrinsic ones introduced in the course of dwelling process of the indenter. Such kind of trend was also reported on vapor grown $Bi_2Te_{3-x}Se_x$ whiskers due to cohesiveness of the atomic layers (Kunjomana and Chandrasekharan. 2008). Large amount of slip rapidly deteriorates the mechanical behavior, (Khanna. 2014), because each region of the sample moves or glides faster over another part of the surface. But the present filamentary crystals of monophase grown under optimized supersaturation are found to be fairly stronger as they are resistant to sliding than other photovoltaic materials, like γ-In_2Se_3, InSe, etc. (Ajayakumar and Kunjomana. 2016, Teena and Kunjomana. 2017). Values of microhardness and the related parameters such as yield strength (Y) and stiffness constant (C_H) are listed in Table 7, which are superior to that of reported in the literature (Reshmi et al. 2011). The estimated Young's modulus (= 69 GPa) is also greater than that of the CdS compound semiconductor (Harsy et al. 1971), which justify the mechanical stability of the grown whiskers.

Table 7: Mechanical characteristics of Sb_2Se_3 whiskers

Load ($\times 10^{-3}$kg)	Hardness (kg/mm^2)	Yield strength (kg/mm^2)	Stiffness constant (10^3 kg/mm^2)
5	158.13	52.71	7.05
10	209.81	69.94	11.57
15	227.52	75.84	13.33
25	249.09	83.03	15.62
35	257.13	85.71	16.51
50	256.98	85.66	16.49
75	256.86	85.62	16.48
100	256.75	85.58	16.47

Electrical characteristics describe the ability of a material to transport carriers by the process of conduction. Hall effect measurements performed at room temperature (25 ºC) showed positive signs for voltage and Hall coefficient, indicating *p*-type conductivity of the as-grown antimony selenide whiskers. The probability of multiphase generation in *p*-type material is less as they require large activation energy to create unwanted phases than the *n*-type samples, thus reducing the formation of recombination centres and enhancing the photogenerated carrier

collection of the crystal. Such research findings were commonly noticed in the binary chalcogenides, for e.g., *n*-In_2S_3 exists in both α as well as β phase along with other mixtures like In_3S_4, In_4S_5, InS, In_2S, etc. (Rehwald and Harbeke, 1965). In order to overcome this complexity, the homemade precursors were used as starting materials for the growth of vapor deposited habits under high vacuum (~ 10^{-6} mbar) and resulted in chemically homogeneous monophase samples (Fig. 17&18, 20 and 21). The resistivity (ρ) was calculated using the formula, $\rho = \frac{R}{Al}$, where *R* is the resistance deduced from the applied current versus voltage plot (Fig. 23), *A* is the cross-sectional area and *l*, the length of the sample. The Sb_2Se_3 samples bearing 0.5 at. % deficient selenium, crystallized from the melt was reported by Bacewicz and Cizek (1991). This deviation in chemical composition led to high resistivity (< 10^5 Ω cm) and enhanced the scattering of charge carriers during the transport process. In the present work, the low value of ρ (145.36 Ω cm) was achieved due to the homogeneity of the whiskers synthesized from stoichiometric ingot (Fig. 20a). Also, the periodic arrangement of atoms in the lattice (Fig. 17& 18b) facilitated attenuation of trap states, which promoted smooth flow of current in the semiconductor.

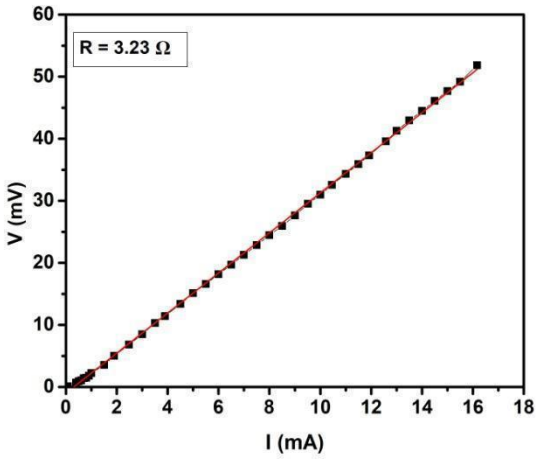

Fig. 23: Current-voltage characteristics of the Sb_2Se_3 whiskers

The values of Hall coefficient (R_H), mobility (μ) and carrier concentration (*n*) were computed as 0.8447 cm^3/C, 5.81 × 10^{-3} cm^2/Vs and 7.39 × 10^{18} cm^{-3} respectively, using the equations $R_H = \frac{V_H d}{IB}$, $\mu = R_H \sigma$ and $n = \frac{1}{R_H q}$, where σ is conductivity, V_H is Hall voltage, *d* is thickness of the

sample and q gives electric charge (1.602×10^{-19} C). The mobility of Sb_2Se_3 whiskers can be associated with the slight scattering of carriers during the transport mechanism. The poorly attached Sb_2Se_3 material on the substrate, with improperly packed large rod-shaped crystallites during chemical vapor deposition, leads to a film of low density and non-uniform thickness, resulting in high resistivity with a very low carrier density of 5.75×10^{11} cm^{-3}(Benjamin et al. 2015). Bacewicz and Cizek (1991) have reported very low value of n ~10^{13} cm^{-1} in the melt crystallized non-homogeneous antimony selenide crystals compared to that (7.39×10^{18} cm^{-3}) of the present vapor deposited stoichiometric samples, which suggests the possibility of the latter for energy conversion.

Conclusions

Diverse habits such as coir-like fibers, whiskers, needles, spherulites, etc. of Sb_2Se_3 were crystallized, employing a cost-effective physical route comprising the sublimation of customized chemically homogenous ingot and subsequent deposition at the growth temperature 560 and 530 °C. Microstructural images captured using electron and optical microscopes, revealed the development of good quality whiskers, bearing low defects, as a result of the successive addition of atoms on the smooth vapor-solid (v-β) interface, as per the KSV model. The powder diffractograms revealed sharp, distinct and prominent peaks due to the strong reinforcement of scattered rays. Furthermore, Rietveld refinement analysis justified the crystal system as orthorhombic, validating the monophase nature of the grown crystals. EDAX provided the elemental proportion, Sb: Se (= 39.98:60.02), close to the right atomic ratio (40: 60), which is compared to that evaluated from XPS analysis. Microhardness studies provided appreciable hardness, stiffness constant and Young's modulus, reflecting mechanically strong crystals, in addition to being thermally stable. The evaluated band gap and absorption coefficients were found to be ~1.15 eV and 2.38×10^5 cm^{-1} respectively. The computed values of resistivity, mobility and carrier concentration are equal to 145.36 Ω cm, 5.81×10^{-3} cm^2/Vs and 7.39×10^{18} cm^{-3}, respectively. The overall research findings thus promise a way to scale up the performance of physical vapor deposited antimony selenide than the other CVD and melt crystallized samples for photovoltaic applications.

4.2 Vapor growth and characterization of $SnSe_2$ crystals

The vapor deposited platelets grown under low supersaturation (S) at ΔT = 270 ºC (nutrient temperature, T_N = 800 ºC and growth temperature, T_G = 530 ºC) result in a rough vapor-solid (v-β) interface that leads to the development of voids in-between the layers, over deposits, kinks, and steps on the crystal surface (Fig. 24a). A small reduction of the temperature in the growth zone from 530 to 520 ºC, facilitated the adequate filling of the gaps formed between the layers, also the extra growth was inhibited (Fig. 24b). This result further justifies that the layer-by-layer growth is the characteristic attribute of the crystallographic hexagonal structures in the absence of external transporting agents. In order to attain an atomically smooth v-β interface the T_G was intestinally reduced to 500 ºC (ΔT = 300 º), the crystalline deposits were observed to have large gains with steps on the topography of the crystal (Fig. 25a). Hence, the periodic atom by atom deposition resulted in the stacking of layers by eliminating the voids and over deposits. On the other hand, George and Kumari (1986) have observed circular as well as hexagonal spirals on the surface of tin diselenide crystals grown by physical vapor transport, indicating the spiral growth mechanism. Also, Wu et al. (2016) have detected the spirals on the $SnSe_2$ platelets surface, synthesized at low supersaturation, due to the screw dislocation-driven growth. These defective sites are the most preferable region for the origin of further new nuclei. Similarly, Verma (1953) clearly accounted that at the low S (= α – 1, where $\alpha = p/p_e$) the steps provided by the screw dislocation will have kinks, and the atoms are adsorbed on the crystal surface they diffuse on the step and finally reach to the kinks where they are adsorbed for further development of the sample, and thus the step advances. Hence in the present work, an attempt was made to develop a smooth v-β interface by modifying the supersaturation to obtain the good quality tin diselenide crystals for photovoltaic application.

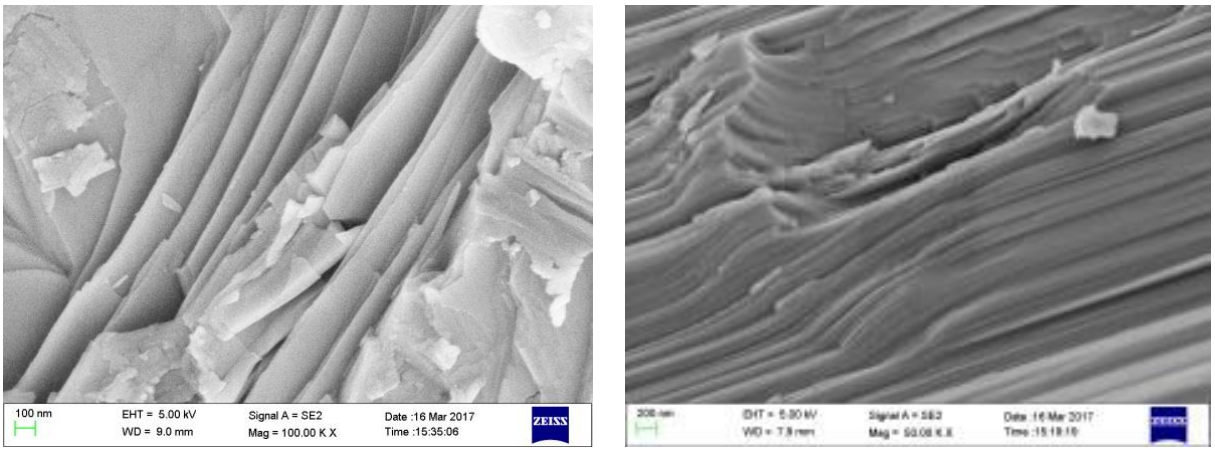

Fig. 24: SEM images of $SnSe_2$platelets grown at (a) $\Delta T = 270$ ºC (b) $\Delta T = 280$ ºC

Liu et al. (2016) experimentally proved that at higher *S*, the $SnSe_2$ crystal exhibits layer-by-layer (LBL) and dendritic growth modes. Therefore a detailed morphological investigation of the as-grown $SnSe_2$ crystals was performed using optical and high resolution electron microscopes, which justifies that the crystal grew by Frank-van der Merwe mechanism as per the per the KVS model (Moorthy, 2015). The observed images substantiated the absence of inclusions, clusters, nodules, dislocations, hillocks, spirals, helical fringes, etc. on the sample surface (Fig. 25a-b). On the other hand, many research groups (George and Kumari, 1986 & Agarwal et al., 1991) synthesized tin diselenide platelets, but observed the defective features on the surface this is may be due to the polytypism. In the present work the physical vapor deposition (PVD) was adopted to grow tin diselenide samples via an indigenously assembled dual zone furnace without any additional transporting agents. The correlation between growth temperature and the morphology of the vapor grown $SnSe_2$ crystals were presented in Table 8.

Table 8: Experimental condition of $SnSe_2$ crystals under different experimental conditions

Temperature (ºC)				
Nutrient Zone (T_N)	Growth Zone (T_G)	Growth period (days)	Temperature difference (ºC)	Morphology
800	530	3	270	Layers with voids and over deposits (Fig. 24a)
800	520	3	280	Kinks and layers (Fig. 24b)
800	500	3	300	Parallel layers with hexagonal platelets (Fig. 25a)
860	460	3	400	Well developed platelets (Fig. 25b)
870	460	3	410	Layered patterns on the platelets (Fig. 26a)
880	460	3	420	Over deposits on the platelets (Fig. 26b)

Agarwal et al. (1991) have grown $SnSe_2$ platelet crystals by chemical vapor transport (CVT) method, with iodine as a transporter. However the surface of the compounds exhibited high roughness. The habit modification in $SnSe_2$ crystals from hexagonal to triangular structures due to the influence of the SiO_2 substrate was reported by Wu et al. (2016). Al-Hilli and Evans (1972) have discussed the different topographical patterns of the molybdenum diselenide ($MoSe_2$) crystals, grown by CVT synthesis route, this is owing to the presence of halogens and carrier gases. In order to overcome these challenges, additional cleaning, solvent treatment or polishing is adopted in those samples grown from CVD/CVT approach. Sunagawa(1999) has reported that the crystals with unit cells of comparable size bear isometric forms and those with size, $a \approx b < c$ easily grew in platy forms. It is interesting to note that the platelet formation was observed in PVD grown $SnSe_2$ crystals with the lattice parameters of the crystals was calculated as, a = 3.811 Å, and c = 6.137 Å. Further modification of growth conditions, ΔT = 400 ºC (T_N = 860 ºC and T_G = 460 ºC) facilitated the periodic deposition of vaporized atoms by the proper rearrangement of crystal lattice to accomplish smooth platelets (Fig. 25b).

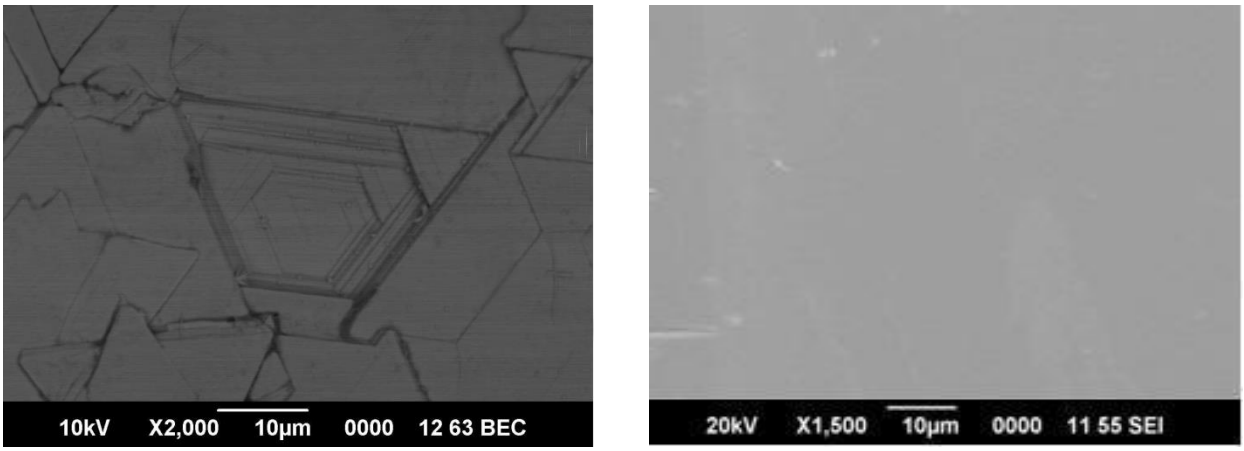

Fig. 25: SEM images of $SnSe_2$ platelets grown at (a-c) ΔT = 300 ºC (d) and ΔT = 400 ºC

The SnSe-$SeSe_2$ composites have grown by directional solidification process using Bridgman-Stockbarger method and possess a high degree of porosity as discussed by Aguiar et al. (1999). The evaporation of constituents during solidification arises due to selenium sublimation or the presence of SeO, SeO_2, SeO_3. These oxides are not stable at melting temperature, which leads to the formation of bubbles. Consequently, the melt grown products exhibit voids. However, such defects were not observed in the vapor grown platelets, which justifies the absence of re-evaporation of constituents and the oxide formation during the crystallization process. At high supersaturation, the surface of the as-grown crystals were found to be several over deposits (Fig. 26a-b) due to the rough vapor-solid interface at ΔT = 410 and 420 ºC. Thus, the electron microscopic findings prove the absence of screw dislocation driven growth in $SnSe_2$ platelet. Therefore, the good quality samples grown at ΔT = 400 ºC were selected for the further physical characterization.

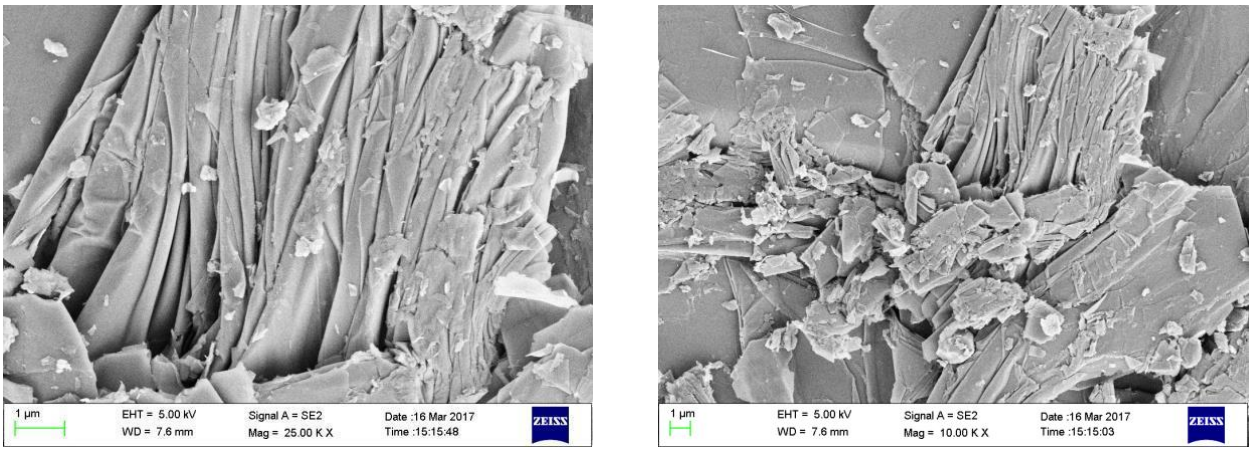

Fig. 26: SEM images of $SnSe_2$ crystals exhibiting over deposits with irregular layer arrangement (a) $\Delta T = 410$ ºC (b) $\Delta T = 420$ ºC

Structural and stoichiometric analysis of $SnSe_2$ platelets

Evaluation of the crystallographic properties like lattice parameters (*a*, *b*, and c), cell volume (*V*) and density (*D*) is necessary to estimate the quality of physically deposited samples. In this regard, powder X-ray diffractogram (PXRD) was utilized to probe the phase and chemical purity of the as-grown crystals. Julien et al. (1992) have reported that the $SnSe_2$ semiconducting material crystallized in a hexagonal close-packed structure is formed by van der Waals bonding between Sn-Se-Sn layers. Tin diselenide platelets grown by spray pyrolysis as discussed by Martinez-Escobar et al. (2013), exhibited a mixture of three phases like $SnSe_2$, SnSe and Se owing to the small variations in solution flow rate, molar concentration and the atomic ratio of the precursor. But in the present work, the vapor deposited by $SnSe_2$ platelets under high vacuum (~ 10^{-6} mbar) possessed monophase, this is supported by the PXRD pattern, which does not indicate the presence of any other phase, such as SnSe, Sn_2O_3, SnO_2, Sn, Se, etc., (Fig. 27a). The periodicity of the atomic deposition was enhanced at $\Delta T = 400$ ºC (Fig. 25b) which grew in the spread of layers promoted by the release of latent heat of energy. All the diffracted peaks in the profile were found to be stronger as compared to the standard data (collection code: 43594), which is due to coherent scattering of atoms from such a large number of similar parallel planes, following the Laue condition of diffraction. In these domains the atoms are arranged along each other up to their equilibrium distances with the decrease in

enthalpy (ΔH), reducing the free energy of the system (ΔG_v) during crystal growth. However the diffractogram shows only six reflections lines from (001), (011), (102), (003), (110) and (004) planes, justifying that the atoms are periodically oriented in the as-grown platelets. Nahass (1992) has grown bulk polycrystalline $SnSe_2$ by mixing the Sn and Se in stoichiometric proportions, but obtained very weak peaks in the PXRD profiles. Minagawa (1980) has reported that the $SnSe_2$ crystal grown from three different approaches like the chemical transport reaction using iodine, melt growth by Kapitza method and sublimation process, exhibited *18R*polytypism (most or second common polytype). The crystal possessed hexagonal crystal structure with lattice parameters of, a = 3.81 Å and c = 55.2 Å. But in the present research work, a hexagonal system (CdI_2 structure type) with lattice parameters, $a = b$ = 3.811 Å and c = 6.137 Å and cell volume, V = 77.191 Å^3 was obtained from the Rietveld refinement pattern of the PXRD data using FullProf Suite software (Fig. 27b), which is in accordance with the standard ICSD data (collection code: 43594). The impurities such as Se or SnSe were not detected, justifying the phase purity or monophase nature of the vapor deposited $SnSe_2$ platelet samples. The diffraction peaks emerged from the samples shows only the hexagonal unit cells rather the mixture of hexagonal and cubic unit cells due to the utilization of homemade stoichiometric initial ingot and the careful optimization of experimental conditions (supersaturation) under high vacuum. The PXRD result was further supported by the selected area electron diffraction (SAED) pattern as obtained from the complementary technique of transition electron microscope (TEM) of the as-grown platelet crystal, indicating the absence of stacking faults related to phase transformation and polytypism. The red color circled portion in the TEM image (Fig. 27c) shows the kink formation during crystallization which further confirms the Frank-van der Merwe growth mechanism. The well defined and intense diffraction spots confirmed the single crystalline nature as well as the quality of the hexagonal vapor grown samples. The planes in the SAED photographs were identified and indexed in the images as depicted in Fig. 27d, in accordance with Zhou et al. (2016). The density of the samples were computed from the PXRD data as per the equation (3),

$$D = \frac{nM}{VN_a} \tag{3}$$

where M &V are the molecular weight as well as the cell volume of the sample and N_a is the

Avogadro's number of the tin diselenide platelets and have been found to be 5.967 g/cm^3. The value is in agreement (D = 5.969 g/cm^3) with the result calculated from the Archimedes principle (density bottle experiment).

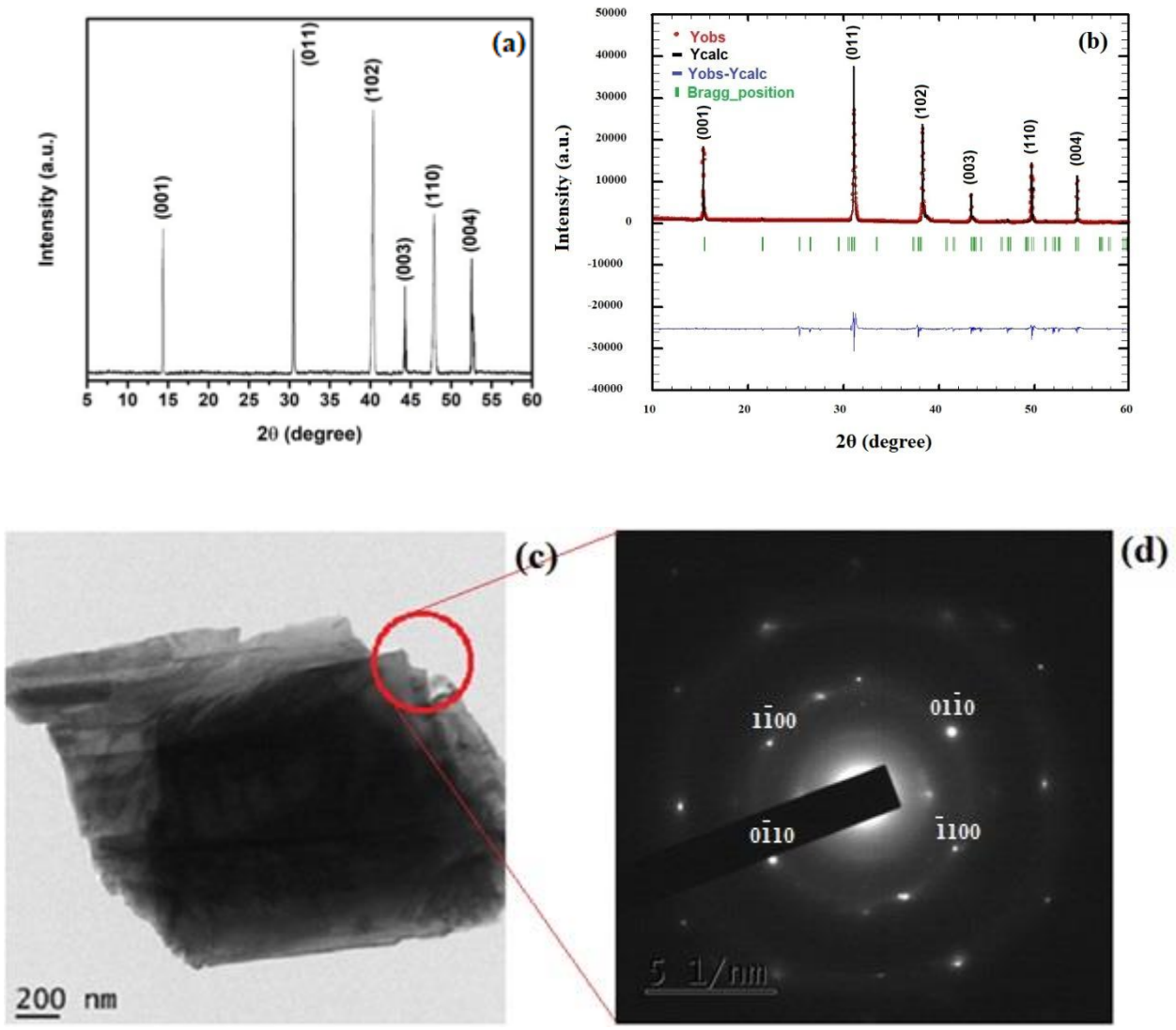

Fig. 27: (a) PXRD profile (b) Rietveld refinement pattern of the same crystallographic data (c) TEM image and (d) SAED pattern of the well-developed $SnSe_2$ platelets

As the optoelectronic properties are governed by structural deficiencies, hence it is essential to probe the occurrence of extraneous materials, secondary phases and non-stoichiometry for optimizing the physical characteristics. The as-deposited $SnSe_2$ samples were

subjected to energy dispersive analysis by X-rays (EDAX) for elemental identification. The atomic proposition of Sn and Se in the synthesized ingot was found to be 33.34 and 66.66 at. % (Fig. 28a) justifying the absence of SnO, SnO_2, Sn_2O_3, SnSe, etc. after repeated trials. The $SnSe_2$ platelets grown by physical vapor deposition exhibit 33.35:66.65 at.% (Sn:Se) as depicted in Fig. 28b, which is close to the standard stoichiometry (33:67). The customized $SnSe_2$ ingot sublimed at $\Delta T = 400$ ºC facilitated the incorporation of atoms in the kink sites by releasing the latent heat of free energy. The harvested crystalline products were properly covered using transparent parafilm tape in order to avoid reactions from the atmosphere. On the other hand, Trifonova et al. (1996) grew $SnSe_2$ crystals by the Bridgman technique followed by purification and further detected a compositional fluctuation of 4 at.%, which is due to less purity of the initial selenium powders. Tin diselenide compounds prepared using iodine vapor transport method exhibited excess tin and iodine on the sample surface in the form of precipitates, which decreased the mobility and increased the resistivity of the carriers as reported by Rimmington et al. (1972). In the present research work, the traces due to excess of constituent elements or any other impurities were not observed, pointing towards the effectiveness of physical vapor deposition performed under high vacuum atmosphere (~ 10^{-6} mbar) for the production of monophase tin diselenide platelets.

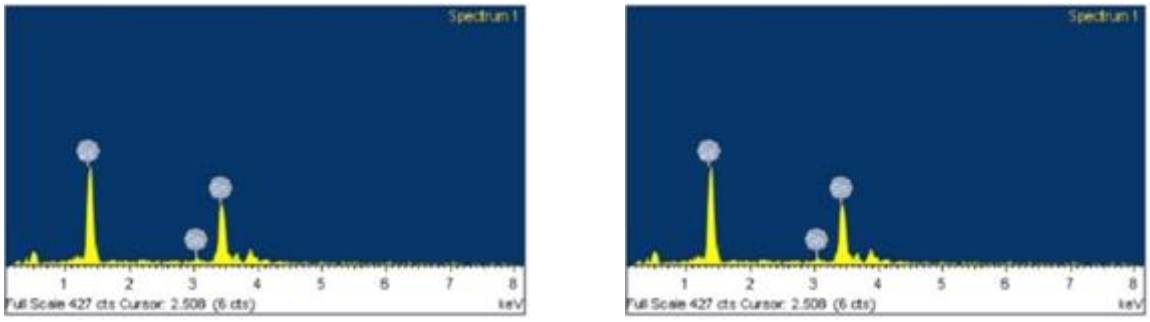

Fig. 28: EDAX profiles of $SnSe_2$ (a) ingot and (b) platelets

X-ray photoelectron spectroscopy (XPS) is an essential characterization tool to determine the nature of chemical bonding, phase and stoichiometry of the samples. The intensity of peaks in the XPS spectrum depends on the number of electrons and their orbital energies being emitted from the crystal surface. The electrons are ejected when incident monochromatic soft X-rays of

Al K_α (1486.6 eV) were absorbed. The prominent oxygen traces in the chemically deposited crystals have been observed in the XPS spectra due to the mica substrate as reported by An et al. (2018). In order to inhibit such kind of oxide formation in the deposited $SnSe_2$ crystals at the elevated temperature during the growth process, high quality quartz ampoules were adopted. The XPS characterization was performed under ultra-high vacuum level with a base pressure of 2×10^{-9} mbar. In the current work, only tin and selenium core levels were found and no peaks corresponding to other contaminants were detected, except carbon (Fig. 29a). The origin of very weak intense carbon (C1s) in the sample surface arose from the adsorption in the ambient environment after growth as discussed by Mandal et al. (2010). The binding energy (BE) is referenced to the C1s peak positioned at 284.6 eV as depicted in Fig. 6b. The quantitative analysis confirmed the right atomic proportion of Sn and Se (33.36:66.64 at.%) in the deposited which can be attributed to the utilization of chemically homogeneous $SnSe_2$ ingot (Fig. 6a) and careful experimental conditions (high vacuum, ultra-fine cleaning of the ampoule etc.). The high-resolution photoemission spectra of the Sn 3d and Se 3d were also performed and depicted in Fig. 29c and d. The energy for Sn $3d_{3/2}$ and Sn $3d_{5/2}$ are located at 496.409 eV and 487.049 eV, respectively (Fig. 29c). The difference between the core level spectra of tin was estimated to be 9.36 eV, which further proved that the prepared platelets were of tin diselenide with the right valence of Sn, crystallized in a hexagonal $SnSe_2$ form. On the other hand, Zhou et al. (2016) observed orthorhombic SnSe, as the oxidation state of Sn was +2. The core-level spectra of the constituent element Se 3d is shown in Fig. 29d, wherein the peak split into two states, Se $3d_{3/2}$ and Se $3d_{5/2}$. The binding energies of 53.784 eV and 54.341 eV corresponding to Se $3d_{3/2}$ and Se $3d_{5/2}$ justify the monophase nature of the as-grown $SnSe_2$ platelets deposited by the PVD method.

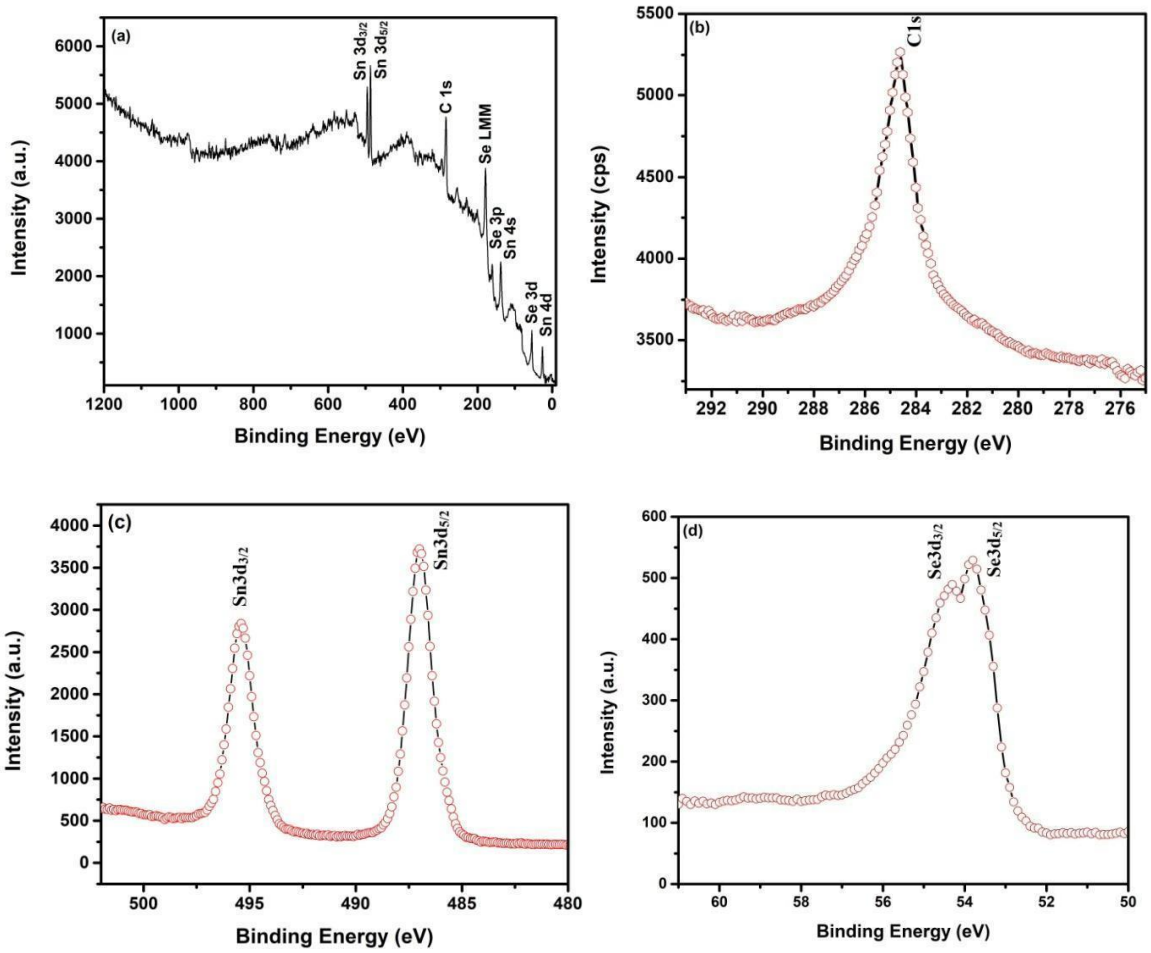

Fig. 29 (a) wide-spectra of $SnSe_2$ platelets, core-level spectra (b) C1s (c) Sn3d and (d) Se3d

Thermal and Mechanical Analysis

Thermogravimetric analysis (TGA) of $SnSe_2$ platelets were carried out in a nitrogen (N) environment from room temperature to 900 ºC using the Perkin Elmer instrument. In order to maintain the controlled environment, a purge gas was continuously flowed through the TGA setup. TGA is a technique where the mass of the material is measured as a function of temperature or time while the sample is subjected to a controlled temperature program. The recorded TGA trace of 5g of platelets is depicted in Fig 30a, the mass loss due to the volatile components such as absorbed moisture and water that generally evaporated between ambient to 300 °C were not detected in the vapor deposited $SnSe_2$ crystals. Also, there was no detectable weight loss before 650 ºC, ensuring the absence of SnSe, SnO_2, Sn and Se formation during the

vapor deposition. Tin diselenide is a layered compound belonging to Sn-Se phase diagram, the prominent mass loss (congruent melting) was observed at (= 650 ºC), which indicates the decomposition of the sample. The $SnSe_2$ platelet crystals showed relatively sharp, well-defined melting points because all the component atoms are an equal distance from the same number and type of neighbors; that is, the regularity of the crystalline lattice creates local environments that are the same. Thus the intermolecular forces holding the solid together are uniform, and the same amount of thermal energy is needed to break every interaction simultaneously (Saha et al. 2016). The sharp weight loss in the TGA curve indicates a high degree of crystallinity and the absence of stacking faults in the vapor deposited sample is in agreement with the PXRD result.

The mechanical parameters of the crystal play a vital role in practical photovoltaic device fabrication. With this notion, the behavior of the as-grown tin diselenide crystals under force was assessed with a diamond indenter using Vickers microindentor (MVH-I) coupled with a computer arrangement (Quantimet software). The PVD grown $SnSe_2$ platelet was mounted on the glass slide along the platform of the hardness tester and loads of different ranges from 5 to 100 g were applied over a constant dwell time interval of 10 s. The variation of hardness number versus load was shown in Fig 30b. The melt grown (Bridgman-Stockbarger) $SnSe_2$ crystals have exfoliated along the cleavage plane under the ice environment for hardness measurement as discussed by Pandya et al. (2011). The fluctuating results (the hardness is decreased load up to 30g and increased for the load above 30g) with very low hardness are reported by the melt grown samples due to the deformation accommodated by dislocations, may be related to the polytypism. From the plot, it is vivid that the hardness value increases with the addition of load up to 100 gm. When the load reaches 50 gm, it is found that the H_v was saturated this is due to the strong covalent bond between the Sn and Se atoms (Kunjomana et al. 2019). Trifonovaet al. (1996) have reported the very low microhardness number (72.80 ± 6.88 kg/mm^2) of the directly synthesized (melt grown) $SnSe_2$ crystals using Bridgman technique at a temperature gradient of 10 °C/cm and ampoule lowering rate of 0.47 mm/h.

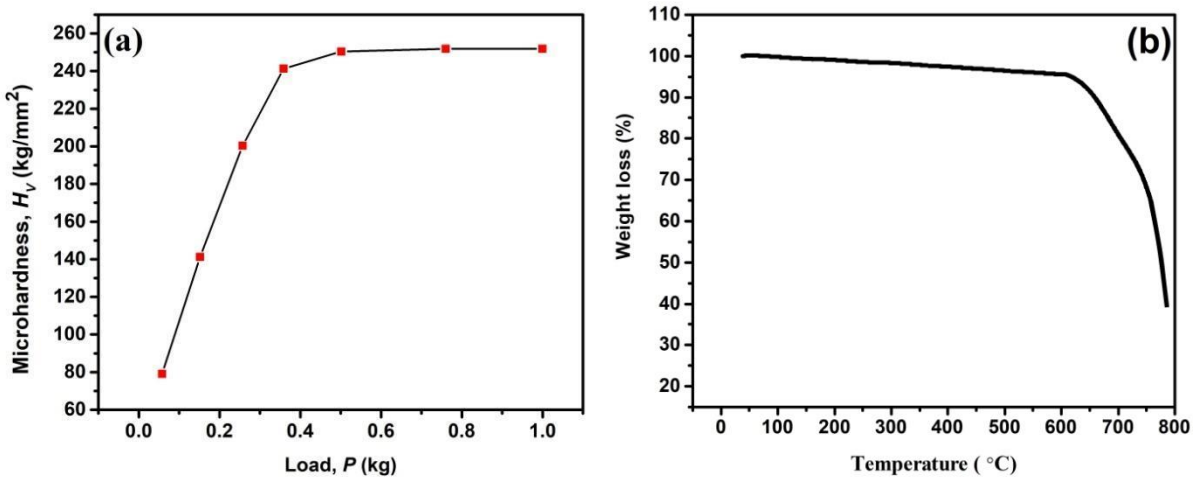

Fig. 30: (a) Plot of load versus microhardness and (b) TGA profile of $SnSe_2$ platelets

The defects such as crack, deformation, etc. were not observed in the vapor grown $SnSe_2$ samples due to the applied force. The elastic stiffness constant (C_H) was calculated using the hardness number with Wooster's empirical relation. The mechanical properties of the vapor deposited tin diselenide platelet were presented in Table 9.

Table 9: Mechanical parameters of $SnSe_2$ platelets

Load ($\times 10^{-3}$kg)	Hardness (kg/mm^2)	Yield strength (kg/mm^2)	Stiffness constant (10^3kg/mm^2)
5	79.05	26.35	2.09
15	141.25	47.08	5.79
25	200.92	66.97	10.72
35	241.31	80.46	14.77
50	250.38	83.46	15.76
75	251.85	83.95	15.92
100	251.87	83.96	15.92

Optoelectronic properties of the $SnSe_2$ platelet crystals

The effective absorption of solar radiation in a crystal represents a complex interaction of light with the semiconductor atomic structure. Such relations lead to the generation of free charge

carriers in the material, electrons and holes, contributing to the transformation of energy carried by light into electrical energy. The formation of photo-generated carriers is a result of breaking of the atomic bonds. The excitation of an electron directly from the valence band (which leaves a hole behind) to the conduction band is the fundamental absorption. The photons must possess a minimum energy equal to the band gap of a semiconductor in order to free an electron from a covalent bond. Electromagnetic radiation with higher energy than the E_g creates electron-hole pairs and the extra energy received from the photons is released as heat into the lattice during the thermalization process. An important key for obtaining an efficient solar cell is to minimize the heat losses due to the temperature by selecting semiconductors with appropriate band gaps. The most effective materials for solar energy conversion must have band gap energies in the range of 1 to 1.8 eV, and $SnSe_2$ binary compound shows an E_g of the order of 1.20 eV. Hence this material serves as a good choice for PV applications. In direct band gap semiconductors, such as GaAs, GaInP, CdTe, and $Cu(InGa)Se_2$, have high absorption coefficient, but these materials also have toxicity, melting temperature, and expensive making them unfavorable for semiconductor industry (Oda. 2007). Both the total energy (*E*) and momentum (*P*) of all particles involved in the absorption process is conserved. Since the *P* of the photon is very small as compared with the range of the crystal the light absorption process effectively conserves the momentum of the electron.

In the present work, the optical data of the as-grown $SnSe_2$ platelets were carried out using a UV-Vis-NIR of model Cary 5000. The optical absorption coefficient (α) was determined (5.8×10^5 cm^{-1}) using the formula, $\alpha = 2.303\, A/t$, where A is the absorbance and t is the thickness of the platelet. Garg et al. (1976) have reported that the direct allowed nature of optical absorption of the vapor grown $SnSe_2$ crystals without the use of any transporting agents exhibited a band gap of 2.1 eV. Even though the former has appreciable E_g, numerous amounts of selenium deficiency were observed. On the other hand, the crystals grown by vertical Bridgman method shows direct transition of 1.28 eV band gap with a *6H*-polytype and a drastic change in the E_g value from 1.28 to 1.40 eV as reported by Powell and Grant (1996). Acharya and Srivastava (1981) discussed the band gap for *2H* and *22H* structures, which is found to be 1.21 and 0.66 eV respectively, for the $SnSe_2$ crystals produced by closed tube transport technique with a small amount of iodine. It is worthwhile to note that the crystals grown from the vapor

phase method using the carrier reagents exhibit an indirect nature of transition with E_g in the order of 0.98 to 1.03 eV as reported by several authors (Bhatt et al. 1989, Julien et al. 1992, Gerorge and Kumari. 1986). Also, these samples bearing spiral, hillocks, precipitates, etc. are defective due to the presence of impurities from the carriers. The core reason behind the transition from indirect to the direct transition of phonon absorption and the variation in the band gap is due to the significant change in the unit cell dimensions associated with the ploytypism as reported by Bechstedt and Belabbes(2013). Figure 31a shows the intercept of the $(\alpha hv)^2$ versus hv, and the direct band gap, E_g, value as 1.20 eV, which was less than that reported for the polytype of $SnSe_2$ hexagonal platelets (1.21 eV) grown by closed tube transport method. In the as-grown $SnSe_2$ platelets, all the atoms in hexagonal unit cells were interlocked in the same way and have the similar orientation resulting in strong overlapping of energy levels and resulting in reduction in band gap. Compared with direct transitions, the absorption coefficient for indirect transitions is relatively small. As a result, light penetrates more deeply into indirect band gap semiconductors than direct (Oda. 2007). In indirect band gap semiconductors such as Si and Ge, where the valence-band maximum occurs at a different crystal momentum from that of the conduction band minimum, conservation of electron momentum necessitates that the photon absorption process involves an additional particle. Hence, phonons are suited to this process because they are low-energy particles with relatively high momentum.

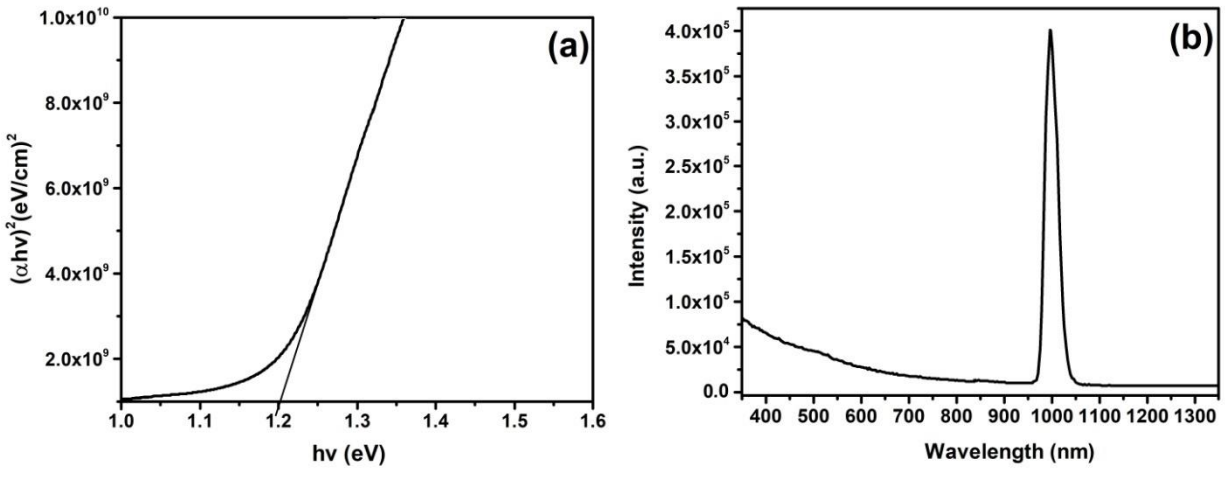

Fig. 8 (a) Tauc plot and (b) PL spectrum of $SnSe_2$ platelets

The minor deviation in stoichiometric ratio or impurity will create an intermediate energy state in the forbidden region, this facilitates the recombination during the transport process. In the present work, the deposited plate-like crystals possess the right chemical homogeneity, excluding the chances of trap states in the crystal. This will improve the absorption of light as well as the transport process of the photogenerated electron-hole pairs. Trap-assisted recombination usually occurs due to the impurities or defects in the materials that result in trap stages (energy levels) in the band gap. Alternatively, if the trap captures a hole from the valence band edge before the captured electron is released to the valence band, then the two carriers will recombine and the trap will be empty again, thus releasing a phonon as the result of the recombination. Hence, for the high performance of optoelectronic devices, the production of pure and non-defective crystals is necessary (Yu et al. 2012). Surface recombination is the annihilation of carriers in the near vicinity of a semiconductor surface via the interaction with interfacial traps. In order to probe the minute presence of impurities, polytypism and optical characteristics, the photoluminescence (PL) spectrum of the vapor deposited samples was recorded at an excitation wavelength of 730 nm. Generally, the front surface of a solar cell has a high concentration of defects due to the abrupt termination of the crystal lattice (dangling bonds), these manifest themselves as a continuum of traps within the forbidden gap at the surface. Kim et al. (1987) reported that the Bridgman growth of α-In_2Se_3 single crystals exhibited two peaks in the PL spectra, of which the luminescence centre originated from intrinsic defects. It was also observed that the recombination region occurred from an extrinsic defect formed by excessive indium and thermal activation energy. The growth of single crystalline indium triselenide is difficult owing to the control of stoichiometric ratio and crystal structure of In_2Se_3 compounds (which possess different α, β and γ phases). The as-grown $SnSe_2$ crystals showed sharp and intense peaks in the infrared region at 1024.49 nm with a band gap equals to 1.21 eV (Fig. 31b) and is comparable to the energy gap calculated from the UV-Vis-NIR data. Moreover the absence of other shoulder or minute peaks in the PL spectrum, further justifies the fact that vapor grown $SnSe_2$ crystals (careful experimental conditions) are devoid of intrinsic or extrinsic defects, foreign elements, polytypism, etc. in accordance with the EDAX, XPS and PXRD results.

Electrical characteristics are greatly influenced by the surface microstructure, stoichiometry, crystallinity, etc. of the grown crystals. Hence, high quality 1.5 cm long tin diselenide platelets were selected for the Hall effect measurements. Four aluminium (Al) point ohmic contacts were deposited on the corners of the as-grown platelets of area, A = 1.5 cm^2. George and Kumari (1986) reported that the vapor deposited in $SnSe_2$ samples possessed inferior electrical properties, resistivity (17 Ω cm) and low carrier concentration (~ 10^{16} cm^{-3}) due to the spiral formation on the sample surface. Mandal et al. (2010) reported that the defects have a potential influence on the electrical properties, which degrades the performance of the crystal. Crystalline $SnSe_2$ samples prepared directly from its elements possessed *n*-type electrical conductivity due to the presence of iodine carrier (Asanabe, 1961). Busch et al. (1961) concluded that the Bridgman grown tin diselnide products possessed *p*-type conductivity with the carrier concentration ~ 10^{18} cm^{-3}. The performance of a semiconducting device depends on the photogenerated charge carriers that are inside the material and cause the electrical currents. The p-type conductivity of the samples was identified from electrical measurements. The resistivity (ρ) was calculated using the equation, $\rho = \frac{RA}{l}$ from the resistance (R) obtained from the current-voltage plot (Fig. 32). The less value of ρ (= 2.70 Ω cm) was obtained owing to the long range periodic arrangement of atoms in the as-grown platelets.

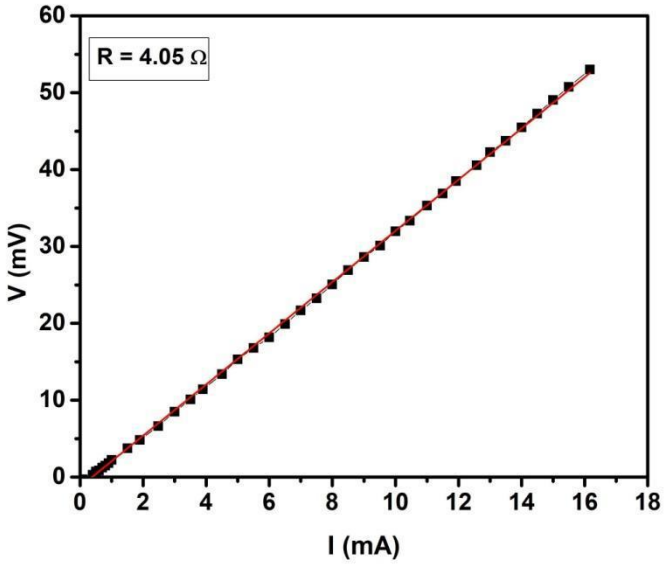

Fig. 32: Current versus voltage of the as-grown $SnSe_2$ platelets

In order to determine the performance of the material, it is important to know the precise number of available charge carriers. Also, the distractions in the motion of free charge carriers due to thermal vibration in the lattice is prominent in the case of indirect semiconductors like Si, Ge and GaP. The concentration of carriers was calculated using the formula, $n = \frac{I}{V_H q} H$, where V_H is Hall voltage, I represents the applied current, H indicates the constant magnetic field, e is electrical charge, n is the number of carriers, and d is the thickness of the sample.

Table 9: Electrical parameters of $SnSe_2$ crystals

Growth method	Resistivity (Ω cm)	Mobility ($cm^2V^{-1} s^{-1}$)	Carrier concentration (cm^{-3})
Physical vapor deposition [present work]	2.70	37.04	6.24×10^{16}
Physical vapor transport (George and Kumari. 1986)	17	36	10^{16}
Chemical vapor transport (Julien et al. 1992)	2.0	18	10^{18}
Melt growth (Bhatt et al. 1989)	1.6	3.35	10^{16}

The estimated carrier density, $n = 6.24 \times 10^{16}$ cm^{-3} and mobility, $\mu = 37.04$ cm^2 V^{-1} s^{-1} of the direct band gap $SnSe_2$ platelets are found to be superior than the results reported by the other melt and vapor methods (Table 9). It justifies that the surface quality of the samples enhanced the transport properties compared to the earlier reports (George and Kumari. 1986, Julien et al. 1992, Bhatt et al. 1989). Thus, the overall research findings open up the possibilities of physically deposited $SnSe_2$ crystals towards photovoltaic energy conversion applications due to the combined effects of long range periodicity, right stoichiometry and monophase nature.

Conclusions

Chemically pure and crystalline tin diselenide ($SnSe_2$) platelets were grown by physical vapor deposition (PVD) method under vacuum environment (~ 10^{-6} mbar) using an indigenously fabricated dual zone furnace. The smooth surface morphology was obtained by the periodic dense deposition of the atoms on the stable nucleus at a constant temperature difference of, ΔT = 400 °C (T_N = 800 °C and T_S = 460 °C). The Rietveld analysis (structure profile refinement) of

the PXRD profiles justified that the as-grown $SnSe_2$ crystallized in hexagonal structure with a = 3.811 Å, c = 6.137 Å, and cell volume = 77.191 $Å^3$. Stoichiometry of the tin diselenide, 40.02:59.98 at.%, was unearthed by EDAX, the result is found to be concurrent with the XPS results. The melting point (~ 650 °C) and mechanical behavior was probed utilizing TGA as well as Vickers microindentation analysis. The band gap (1.21 eV), absorption coefficient (7.25 × 10^5 cm^{-1}), resistivity (2.70 Ω cm), mobility (37.04 $cm^2V^{-1}s^{-1}$) and carrier concentration (6.242 × 10^{16} cm^{-3}) have been estimated using UV-Vis-NIR, photoluminescence and Hall effect techniques. The optimum structural, chemical, mechanical, thermal, and optoelectronic properties of the physically deposited stoichiometric $SnSe_2$ platelets without any notable surface defects pave the way towards the enhancement in the performance of photovoltaic applications.

Melt growth of crystals

Stoichiometric bulk antimony selenide and tin diselenide crystals have been grown by the horizontal normal freezing method and characterized by SEM, PXRD, EDAX, etc. analysis. Physically distinct and chemically homogeneous samples were engineered by controlling the temperature gradient, supercooling and slow cooling. The mechanical parameters of the melt grown cleaved samples were found to be inferior to the vapor deposited Sb_2Se_3 and $SnSe_2$ due to the strong chemical bonding between the neighbouring atoms and proper internal atomic arrangement. The E_g of the melt grown Sb_2Se_3 and $SnSe_2$ crystals were calculated and the values of the order of, 1.23 and 1.27 eV, respectively. Hall coefficient remained positive for both these crystals, indicating *p*-type conductivity and the electrical resistivity was computed as 158.47 Ω cm and 15.36 Ω cm. As the structural, mechanical and optoelectronic properties of the cleaved melt grown materials are inferior to the as-grown crystals; these samples are not suitable for photovoltaic energy harvesting applications.

5 Summary and future work

Summary of the research work

Physical vapor deposition of antimony triselenide crystalline habits was carried out in an indigenously fabricated dual zone furnace by optimizing the supersaturation under high vacuum, without the use of any transporting agents. The diverse morphological features of crystal were produced by stabilizing the temperature difference between the hot and cold zones, ΔT = 130-60 °C, with the aid of a programmable temperature controller mechanism. The electronmicroscopic (SEM and HRTEM) characterizations revealed layer growth mechanism based on the KSV model. The chemical homogeneity, quality and crystalline nature of the PVD grown sphere-like morphologies were confirmed by EDAX, XPS, Raman, and PXRD analyses. Among the various habits, the energy gap estimated by UV-Vis-NIR analysis is highest for these crystals (1.75 eV), probably due to quantum confinement. Furthermore, photoluminescence data corroborates with the optical characterization recorded by UV-Vis-NIR spectroscopy. The overall research findings pave the way for the improvement of the characteristics of the physical vapor deposited samples than those prepared by chemical synthesis routes.

Crystal growth process was further carried out in order to attain the bulk stoichiometric Sb_2Se_3 crystals such as coir-like fibers, whiskers, needles, spherulites, etc. using physical vapor deposition by optimizing the mass transfer in terms of ΔT (= 125 to 350 °C), free of foreign elements and contamination by facilitating the progression of vapor-solid (v-β) interface. Microstructural images captured using electron and optical microscopes justified the development of good quality whiskers owing to the layer growth mechanism as per the KSV model. The superior results of hardness, stiffness constant and Young's modulus promise that the as-grown crystals are thermally stable and mechanically stronger than the corresponding melt crystallized samples. The powder diffractograms revealed sharp, distinct and prominent peaks due to the reinforcement of scattered rays so as to get strong diffractions from the orthorhombic system. PXRD, EDAX and XPS analyses confirmed phase purity and chemical homogeneity of the whiskers. The evaluated values of band gap and absorption coefficients were found to be ~1.15 eV and 2.38×10^5 cm^{-1} respectively. The computed values of resistivity, mobility and

carrier concentration are equal to 145.36 Ω cm, 5.81 × 10^{-3} cm^2/Vs and 7.39 × 10^{18} cm^{-3}, respectively. The overall research findings thus promise a way to scale up the performance of vapor deposited antimony selenide for photovoltaic applications.

Chemically pure and crystalline tin diselenide ($SnSe_2$) platelets were grown by physical vapor deposition (PVD) method under vacuum environment (~ 10^{-6} mbar) using an indigenously fabricated dual zone furnace. The smooth surface morphology was obtained by the periodic dense deposition of the atoms on the stable nucleus at constant temperature difference of, ΔT = 200 °C (T_N = 800 °C and T_S = 600 °C). The Rietveld analysis (structure profile refinement) of the PXRD profiles justifies that the as-grown $SnSe_2$ crystallized in hexagonal structure with a = 3.811 Å, c = 6.137 Å, and cell volume of, 77.191 $Å^3$ with a CdI_2, type C_6, lattice structure. Stoichiometry of the tin diselenide, 40.02:59.98 at.%, was unearthed by EDAX, the result is found to be concurrent with the XPS data. The melting point (~ 650 °C) and mechanical behavior was probed utilizing TGA as well as Vickers microindentation analysis. The band gap (1.21 eV), absorption coefficient (7.25 × 10^5 cm^{-1}), resistivity (2.70 Ω cm), mobility (37.04 $cm^2V^{-1}s^{-1}$) and carrier concentration (6.242 × 10^{16} cm^{-3}) have been estimated using UV-Vis-NIR, photoluminescence and Hall effect techniques. The optimum structural, chemical, mechanical, thermal, and optoelectronic properties of the physically deposited stoichiometric $SnSe_2$ platelets without any notable surface defects pave the way for the enhancement in the performance of energy conversion application.

Stoichiometric bulk antimony selenide and tin diselenide crystals have been grown by the horizontal normal freezing method and characterized by SEM, PXRD, EDAX, etc. analysis. Physically distinct and chemically homogeneous samples (39.96:60.04 at.%for Sb_2Se_3 and 33.37:66.63 at.% for $SnSe_2$) were engineered by controlling the temperature gradient, supercooling and cooling rates. The mechanical parameters of the melt grown cleaved samples (under nitrogen atmosphere) were found to be inferior to the vapor deposited Sb_2Se_3 and $SnSe_2$, due to the weak chemical bonding between the neighboring atoms and proper internal atomic arrangement. The optical and electrical parameters were computed from the UV-Vis-NIR and Hall effect studies. The band gap (E_g = 1.23 and 1.27 eV) and high resistivity (ρ = 158.47 Ω cm

and 15.36 Ω cm) of the melt crystallized sample were found to be inferior to the vapor grown counterparts. The structural, mechanical and optoelectronic properties of the cleaved melt grown materials are lower than the as-grown crystals; these samples are not suitable for photovoltaic energy harvesting applications.

Future Prospects

The adopted growth technique, physical vapor deposition is an efficient tool to engineer novel antimony selenide and tin diselenide compound crystalline structures with improved functionality for photovoltaic applications. The executed research work concerning habit modification is beneficial for further advanced studies under a controlled environment. Thus, studies on the growth and characterization of Sb_2Se_3 and $SnSe_2$ layered chalcogenide materials pave the way for optimizing the material properties to enhance solar cell performance. Hence, the grown layered chalcogenide crystals can be utilized for the fabrication of *p-n* hetrojunction devices for photovoltaic applications.

6 Plan of the thesis

The thesis chapters are organised into six chapters. Chapter 1 introduces the review of photovoltaic materials, different theories of nucleation, growth mechanism and techniques are explained. This chapter also explains the physical properties and objectives of the present research problem. Chapter 2 describes the experimental methodology for the growth of crystals by horizontal normal freezing (HNF) and physical vapor deposition (PVD) processes. A brief account of selected characterization tools is also included in the chapter.

Detailed descriptions of the morphological evolution, growth mechanism and compositional, structural and optoelectronic properties of the Sb_2Se_3 crystalline habits are presented in chapter 3. Chapter 4 deals with the vapor growth and physical properties of $SnSe_2$ platelet crystals for photovoltaic applications.

Chapter 5 reports the growth of antimony selenide through melt solidification and a detailed analysis of the cleaved samples structure, morphology, composition, mechanical parameters and optoelectronic. Results and conclusions of the overall research findings and the scope of the future work are summarised in chapter 6.

Bibliography

Acharya, S. and Srivastava, O.N., 1981. Occurrence of polytypism in $SnSe_2$. Journal of Crystal Growth, 55(2), pp.395-397.

Afzaal, M. and O'Brien, P., 2006. Recent developments in II–VI and III–VI semiconductors and their applications in solar cells. Journal of Materials Chemistry, 16(17), pp.1597-1602.

Agarwal, M.K., Patel, P.D. and Patel, S.S., 1991. Growth of large size single crystals of $SnSe_2$ using a direct transport method. Journal of crystal growth, 110(3), pp.553-558.

Ajayakumar, C.J. and Kunjomana, A.G., 2016. Sublimation process and physical properties of vapor grown γ-In_2Se_3 platelet crystals. Journal of Crystal Growth, 453, pp.99-105.

Al-Hamdi, T.K., McPherson, S.W., Swain, S.K., Jennings, J., Duenow, J.N., Zheng, X., Albin, D.S., Ablekim, T., Colegrove, E., Amarasinghe, M. and Ferguson, A., 2020. CdTe synthesis and crystal growth using the high-pressure Bridgman technique. Journal of Crystal Growth, 534, p.125466.

Al-Hilli, A.A. and Evans, B.L., 1972. The preparation and properties of transition metal dichalcogenide single crystals. Journal of Crystal Growth, 15(2), pp.93-101.

Arivuoli, D., Gnanam, F.D. and Ramasamy, P., 1988. Growth and microhardness studies of chalcogneides of arsenic, antimony and bismuth. Journal of materials science letters, 7(7), pp.711-713.

Arnberg, L., Di Sabatino, M. and Øvrelid, E.J., 2012. State-of-the-art growth of silicon for PV applications. Journal of crystal growth, 360, pp.56-60.

Bacewicz, R. and Ciszek, T.F., 1991. Liquid encapsulated crystal growth and electrical properties of Sb_2Se_3 and Bi_2S_3. Journal of crystal growth, 109(1-4), pp.133-136.

Benjamin, S.L., De Groot, C.H., Hector, A.L., Huang, R., Koukharenko, E., Levason, W. and Reid, G., 2015. Chemical vapour deposition of antimony chalcogenides with positional and orientational control: precursor design and substrate selectivity. Journal of Materials Chemistry C, 3(2), pp.423-430.

Bhatt, V.P., Gireesan, K. and Pandya, G.R., 1989. Growth and characterization of SnSe and $SnSe_2$ single crystals. Journal of Crystal growth, 96(3), pp.649-651.

Bibin, J. and Kunjomana, A.G., 2019. Facile synthesis of novel antimony selenide nanocrystals with hierarchical architecture by physical vapor deposition technique. Journal of Applied Crystallography, 52(2), pp.312-321.

Black, J., Conwell, E.M., Seigle, L. and Spencer, C.W., 1957. Electrical and optical properties of some $M_{2v-b}N_{3vi-b}$ semiconductors. *Journal of Physics and Chemistry of Solids*, *2*(3), pp.240-251.

Boscher, N.D., Carmalt, C.J., Palgrave, R.G. and Parkin, I.P., 2008. Atmospheric pressure chemical vapour deposition of SnSe and $SnSe_2$ thin films on glass. Thin solid films, 516(15), pp.4750-4757.

Brenner, S.S., 1958. Growth and Properties of" Whiskers" Further research is needed to show why crystal filaments are many times as strong as large crystals. Science, 128(3324), pp.569-575.

Chattopadhyay, K.K., 2009. Introduction To Nanoscience And Nenotechnology. PHI Learning Pvt. Ltd.

Garg, A.K., Agnihotri, O.P., Jain, A.K. and Tyagi, R.C., 1976. Optical absorption spectrum of tin diselenide single crystals. Journal of applied physics, 47(3), pp.997-1000.

George, J. and Kumari, C.V., 1986. Optical, electrical and morphological studies of $SnSe_2$ crystals grown by physical vapour transport method. Crystal Research and Technology, 21(2), pp.273-278.

Ghosh, G., 1993. The Sb-Se (antimony-selenium) system. Journal of phase equilibria, 14(6), pp.753-763.

Gibson, E.A. ed., 2019. Solar Energy Capture Materials. Royal Society of Chemistry.

Harsy, M., Balázs, J., Sviszt, P., Pödör, B. and Lendvay, E., 1971. Growth and some physical properties of non-stoichiometric CdS single crystals. Journal of Crystal Growth, 9, pp.209-216.

Hobson, T.D., Hutter, O.S., Birkett, M., Veal, T.D. and Durose, K., 2018, June. Growth and characterization of Sb 2 Se 3 single crystals for fundamental studies. In 2018 IEEE 7th World Conference on Photovoltaic Energy Conversion (WCPEC)(A Joint Conference of 45th IEEE PVSC, 28th PVSEC & 34th EU PVSEC) (pp. 0818-0822). IEEE.

Jabbour, L., Chaussy, D., Eyraud, B. and Beneventi, D., 2012. Highly conductive graphite/carbon fiber/cellulose composite papers. Composites science and technology, 72(5), pp.616-623.

Julien, C., Eddrief, M., Samaras, I. and Balkanski, M., 1992. Optical and electrical characterizations of SnSe, SnS_2 and $SnSe_2$ single crystals. Materials Science and Engineering: B, 15(1), pp.70-72.

Khanna O P, “Materials Science and Metallurgy”, Dhanpat Rai Publications (P) Ltd. New Delhi, (2014).

Kivambe, M., Aissa, B. and Tabet, N., 2017. Emerging technologies in crystal growth of photovoltaic silicon: progress and challenges. Energy Procedia, 130, pp.7-13.

Kunjomana, A.G., Bibin, J., Karthikeyan, R. and Varadharajaperumal, S., 2019. Effect of supercooling on the microstructural development and optimization of physical properties of melt grown SnSe crystals. Journal of Materials Science: Materials in Electronics, 30(15), pp.14300-14311.

Kunjomana, A.G., Bibin, J., Varadharajaperumal, S. and Teena, M., 2021. Control of physical vapor deposition and architecture of stoichiometric SnSe heterojunction structures for solar cells. Vacuum, 191, p.110372.

Kunjomana, A.G. and Chandrasekharan, K.A., 2008. Dislocation and microindentation analysis of vapour grown $Bi_2Te_{3-x}Se_x$ whiskers. Crystal Research and Technology: Journal of Experimental and Industrial Crystallography, 43(6), pp.594-598.

Leng, Y., 2009. Materials characterization: introduction to microscopic and spectroscopic methods. John Wiley & Sons.

Liang, G.X., Zheng, Z.H., Fan, P., Luo, J.T., Hu, J.G., Zhang, X.H., Ma, H.L., Fan, B., Luo, Z.K. and Zhang, D.P., 2018. Thermally induced structural evolution and performance of Sb2Se3 films and nanorods prepared by an easy sputtering method. Solar Energy Materials and Solar Cells, 174, pp.263-270.

Liu, J., Huang, Q., Qian, Y., Huang, Z., Lai, F., Lin, L., Guo, M., Zheng, W. and Qu, Y., 2016. Screw dislocation-driven growth of the layered spiral-type SnSenanoplates. Crystal Growth & Design, 16(4), pp.2052-2056.

Liu, X., Chen, J., Luo, M., Leng, M., Xia, Z., Zhou, Y., Qin, S., Xue, D.J., Lv, L., Huang, H. and Niu, D., 2014. Thermal evaporation and characterization of Sb2Se3 thin film for substrate Sb_2Se_3/CdS solar cells. ACS applied materials & interfaces, 6(13), pp.10687-10695.

Ma, J., Wang, Y., Wang, Y., Chen, Q., Lian, J. and Zheng, W., 2009. Controlled synthesis of one-dimensional Sb2Se3 nanostructures and their electrochemical properties. The Journal of Physical Chemistry C, 113(31), pp.13588-13592.

Mandal, K.C., Hayes, T., Muzykov, P.G., Krishna, R., Das, S., Sudarshan, T.S. and Ma, S., 2010, September. Characterization of gallium telluride crystals grown from graphite crucible. In Hard X-Ray, Gamma-Ray, and Neutron Detector Physics XII (Vol. 7805, p. 78050Q). International Society for Optics and Photonics.

Manivannan, J., Kalaiselvan, S. and Padmavathi, R., 2020. Vapor-Grown Carbon Fiber Synthesis, Properties, and Applications. In Composite and Nanocomposite Materials-From Knowledge to Industrial Applications. IntechOpen.

Martins, D., Stelzer, T., Ulrich, J. and Coquerel, G., 2011. Formation of crystalline hollow whiskers as relics of organic dissipative structures. Crystal growth & design, 11(7), pp.3020-3026.

Mehta, R.J., Karthik, C., Jiang, W., Singh, B., Shi, Y., Siegel, R.W., Borca-Tasciuc, T. and Ramanath, G., 2010. High electrical conductivity antimony selenide nanocrystals and assemblies. Nano letters, 10(11), pp.4417-4422.

Minagawa, T., 1980. Common polytypes of SnS_2 and $SnSe_2$. Journal of the Physical Society of Japan, 49(6), pp.2317-2318.

Nguyen, R.H., 1998. Gallium arsenide. Its uses in photovoltaic applications. IEEE Potentials, 17(5), pp.33-35.Norton, K.J., Alam, F. and Lewis, D.J., 2021. A Review of the Synthesis, Properties, and Applications of Bulk and Two-Dimensional Tin (II) Sulfide (SnS). Applied Sciences, 11(5), p.2062.

Oda O, "*Compound Semiconductor Bulk Materials and Characterization"*, World Scientific Publishing Co. Pte. Ltd., Singapore, 2007.

Ota, J. and Srivastava, S.K., 2010. Synthesis and optical properties of Sb_2Se_3nanorods. Optical Materials, 32(11), pp.1488-1492.

Pamplin B R, “Crystal Growth”, Hungary: Pergamon, 1975.

Pandya, G.R., Vyas, S.M., Shah, R.C. and Shah, N.R., 2001. Study of knoop hardness of tin chalcogenides.

Pillai S O, Solid State Physics, Wiley Eastern Ltd., (1994).

Powell, M.J. and Grant, A.J., 1977. The effect of pressure on the optical-absorption edge in SnS_2 and $SnSe_2$. Il NuovoCimento B (1971-1996), 38(2), pp.486-495.

Pham, A.T., Vu, T.H., Nguyen, Q.V., Vu, M.T., Park, J.H., Park, S.D. and Cho, S., 2021. Br-Doped *n*-Type $SnSe_2$: Single-Crystal Growth and Thermoelectric Properties. ACS Applied Energy Materials, 4(3), pp.2908-2913.

Qi, L., Cölfen, H., Antonietti, M., Li, M., Hopwood, J.D., Ashley, A.J. and Mann, S., 2001. Formation of $BaSO_4$fibres with morphological complexity in aqueous polymer solutions. Chemistry–A European Journal, 7(16), pp.3526-3532.

Reddy, K.R., Reddy, N.K. and Miles, R.W., 2006. Photovoltaic properties of SnS based solar cells. Solar energy materials and solar cells, 90(18-19), pp.3041-3046.

Rehwald, W. and Harbeke, G., 1965. On the conduction mechanism in single crystal β-indium sulfide In_2S_3. Journal of Physics and Chemistry of Solids, 26(8), pp.1309-1324.

Reshmi, P.M., Kunjomana, A.G. and Chandrasekharan, K.A., 2011. Spherulitic crystallization of β-In_2Te_3 by physical vapour deposition. Crystal Research and Technology, 46(2), pp.153-158.

Rimmington, H.P.B., Balchin, A.A. and Tanner, B.K., 1972. Nearly perfect single crystals of layer compounds grown by iodine vapour-transport techniques. Journal of Crystal Growth, 15(1), pp.51-56.

Sangwal K, "Additives and Crystallization Processes from Fundamentals to Applications", John Wiley & Sons, Ltd. 2007.

Schöneich, M., Schmidt, M.P. and Schmidt, P., 2010. Chemical vapour transport of bismuth and antimony chalcogenides M_2Q_3 (M= Sb, Bi, Q= Se, Te).

Shan, K., Zhai, F., Yi, Z.Z., Yin, X.T., Dastan, D., Tajabadi, F., Jafari, A. and Abbasi, S., 2021. Mixed conductivity and the conduction mechanism of the orthorhombic CaZrO3 based materials. Surfaces and Interfaces, 23, p.100905.

Shimada, T., Ohuchi, F.S. and Parkinson, B.A., 1992. Thermal decomposition of SnS_2 and $SnSe_2$: Novel molecular-beam epitaxy sources for sulfur and selenium. Journal of Vacuum Science & Technology A: Vacuum, Surfaces, and Films, 10(3), pp.539-542.

Smith, B.A., Cowlam, N. and Shamah, A.M., 1979. The crystal growth and atomic structure of $As_2(Se, S)_3$ compounds. Philosophical Magazine B, 39(2), pp.111-132.

Sunagawa. I, "Crystals: Growth, Morphology and perfection", New York: Cambridge, 2005.

Tan, G.L., Tang, D., Dastan, D., Jafari, A., Silva, J.P. and Yin, X.T., 2021. Effect of heat treatment on electrical and surface properties of tungsten oxide thin films grown by HFCVD technique. Materials Science in Semiconductor Processing, 122, p.105506.

Teena, M. and Kunjomana, A.G., 2017. Grain-growth engineering and mechanical properties of physical-vapour-deposited InSe platelets. Journal of Applied Crystallography, 50(4), pp.1125-1132.

Tiwari, K.J., Ren, M.Q., Vajandar, S.K., Osipowicz, T., Subrahmanyam, A. and Malar, P., 2018. Mechanochemical bulk synthesis and e-beam growth of thin films of Sb_2Se_3 photovoltaic absorber. Solar Energy, 160, pp.56-63.

TrifonovaE, Yanchev I Y, Manou P, Kambas K, and Anagnostopoulos A N, "Growth and characterization of $SnSe_2$", Journal of materials science, vol. 31, p.3647, 1996.

Trivedi, S.B. and Bhatt, V.P., 1976. Growth of Se—Te whisker crystals from the vapour phase. Journal of Crystal Growth, 32(2), pp.227-232.

Vadapoo, R., Krishnan, S., Yilmaz, H. and Marin, C., 2011. Electronic structure of antimony selenide (Sb_2Se_3) from GW calculations. physica status solidi (b), 248(3), pp.700-705.

Varma A R, "Crystal Growth and Dislocations", Butterwort, London, 1953.

Wang, D., Yu, D., Shao, M., Xing, J. and Qian, Y., 2003. Growth of Sb_2Se_3 whiskers via a hydrothermal method. Materials chemistry and physics, 82(3), pp.546-550.

Wang, H., Zhu, J.M., Zhu, J.J., Yuan, L.M. and Chen, H.Y., 2003. Novel microwave-assisted solution-phase approach to radial arrays composed of prismatic antimony trisulfide whiskers. Langmuir, 19(26), pp.10993-10996.

Wang, Q., Puntambekar, A. and Chakrapani, V., 2016. Vacancy-induced semiconductor–insulator–metal transitions in nonstoichiometric nickel and tungsten oxides. Nano Letters, 16(11), pp.7067-7077.

Wang, X., Cai, K. and Liu, H., 2011. Novel gas-induced-reduction route to chalcogenide nanostructures taking Sb_2Se_3 as an example. Crystal growth & design, 11(11), pp.4759-4767.

Wu, H.J., Lee, P.C., Chiu, F.Y., Chen, S.W. and Chen, Y.Y., 2015. Self-assisted nucleation and growth of [010]-oriented Sb_2Se_3 whiskers: the crystal structure and thermoelectric properties. Journal of Materials Chemistry C, 3(40), pp.10488-10493.

Wu, J., Hu, Z., Jin, Z., Lei, S., Guo, H., Chatterjee, K., Zhang, J., Yang, Y., Li, B., Liu, Y. and Lai, J., 2016. Spiral growth of $SnSe_2$ crystals by chemical vapor deposition. Advanced Materials Interfaces, 3(16), p.1600383.

Yang R B, Bachmann J, Pippel E, Berger A, Woltersdorf J, Gösele U, and Nielsch K, Adv. Mater. vol. 21, p. 3170, 2009.

Yin, P., Shi, Z., Sun, L., Xie, P., Dastan, D., Sun, K. and Fan, R., 2021. Improved breakdown strengths and energy storage properties of polyimide composites: The effect of internal interfaces of C/SiO_2 hybrid nanoparticles. Polymer Composites, 42(6), pp.3000-3010.

Yin, X. and Wang, X., 2016. Kinetics-driven crystal facets evolution at the tip of nanowires: a new implementation of the Ostwald-Lussac law. Nano Letters, 16(11), pp.7078-7084.

Yu, Y., Wang, R.H., Chen, Q. and Peng, L.M., 2006. High-quality ultralong Sb2Se3 and Sb2S3 nanoribbons on a large scale via a simple chemical route. The Journal of Physical Chemistry B, 110(27), pp.13415-13419.

Mavlonov, A., Razykov, T., Raziq, F., Gan, J., Chantana, J., Kawano, Y., Nishimura, T., Wei, H., Zakutayev, A., Minemoto, T. and Zu, X., 2020. A review of Sb2Se3 photovoltaic absorber materials and thin-film solar cells. Solar Energy, 201, pp.227-246.

Zhou, X., Zhang, Q., Gan, L., Li, H., Xiong, J. and Zhai, T., 2016. Booming development of group IV–VI semiconductors: fresh blood of 2D family. Advanced science, 3(12), p.1600177.

Zhigadlo, N.D., 2013. Growth of whisker-like and bulk single crystals of PrFeAs (O, F) under high pressure. Journal of crystal growth, 382, pp.75-79.

LIST OF PUBLICATIONS

Research papers published in national and international journals

1. **Bibin John**, A. G. Kunjomana and Teena Mathew "Vapor Growth and Optimization of Supersaturation for Tailoring thePhysical Properties of Stoichiometric Sb_2Se_3 Crystalline Habits," *Journal of Materials Science: Materials in Electronics* (Springer), 2020, (**IF: 2.478**)

2. **Bibin John** and A. G. Kunjomana, "Facile synthesis of novel antimony selenide nanocrystals with hierarchical architecture by physical vapor deposition technique," *Journal of Applied Crystallography*, vol. **52**, p. 312, 2019. (**IF: 3.304**)

3. **Bibin John**, A. G. Kunjomana and Teena Mathew "Vapor Deposition and Enhancement of Optoelectronic Properties of $SnSe_2$ Platelets," *Journal of Materials Science: Materials in Electronics* (Springer), 2022, (**IF: 2.478**) - communicated

Papers Presented in Seminars/Conferences:

1. **Bibin John,** A. G. Kunjomana and Teena Mathew, "Studies on the Structural Characteristics of Tin Chalcogenide Crystals", National Virtual Conference on Recent Advances in Materials Science (NVCRAMS-2021), October, 7-8, 2021, St. Peter's Institute of Higher Education and Research

2. **Bibin John,** A. G. Kunjomana and Teena Mathew, "Control of Phase Transition on the Structural Properties of Sb-Se System", International Virtual Conference on Materials Research (IVCMR-21), August, 26-27, 202. Easwari Engineering College (Autonomous)

3. **Bibin John** and A G Kunjomana, "Growth and Characterization of Sb_2Se_3 Needle Shaped Crystals", International Workshop on Emerging Trends in Crystal Growth (IWETCG-2020), February, 17, 2020, Government Arts College for Men

4. **Bibin John** and A. G. Kunjomana, “Investigations on Thermodynamical Parameters of Vapor Grown Antimony Selenide Crystals”, International Conference on Advances in Chemical and Materials Science, October 17-19, 2019, Mangalore University